Glycolytic Metabolism of Macrophages Differs by Spatial Location and Subset in Tuberculous Granulomas

by

Victoria Gould

BS Biology, The Pennsylvania State University, 2015

Submitted to the Graduate Faculty of the

Department of Infectious Diseases and Microbiology

Graduate School of Public Health in partial fulfillment

of the requirements for the degree of

Master of Science

University of Pittsburgh

2020

UNIVERSITY OF PITTSBURGH

GRADUATE SCHOOL OF PUBLIC HEALTH

This thesis was presented

by

Victoria Gould

It was defended on

May 26, 2020

and approved by

Robbie B. Mailliard, PhD, Assistant Professor, Infectious Diseases and Microbiology, Graduate School of Public Health, University of Pittsburgh

Carolyn J. Anderson, PhD, Professor of Medicine, School of Medicine, University of Pittsburgh

Thesis Advisor: Joshua T. Mattila, PhD, Assistant Professor, Infectious Diseases and Microbiology, Graduate School of Public Health, University of Pittsburgh

Glycolytic Metabolism of Macrophages Differs by Spatial Location and Subset in Tuberculous Granulomas

Victoria Ann Gould, MS

University of Pittsburgh, 2020

Abstract

Tuberculosis (TB), caused by infection with M*ycobacterium tuberculosis* (Mtb), triggers the formation of granulomas in the host. Granulomas are composed of many different types of host immune cells including T and B lymphocytes, macrophages, and neutrophils (PMN). The metabolic pathways used by immune cells in granulomas are important for cell function and glycolytic metabolic pathways in granulomas may be involved limiting or promoting disease. By understanding immunometabolism in TB granulomas, we can improve diagnosis and potentially create new therapeutics to combat TB disease. GLUT1 is a glucose transporter that transports glucose into the cell. To determine what cell subsets express GLUT1 in a granuloma, IHC was performed on lung granuloma-containing tissue sections from non-human primates (NHP) that were experimentally infected with Mtb. These slides were stained for macrophage markers including CD11c and CD163, and GLUT1, before being imaged by fluorescence microscopy. Image analysis was performed using ImageJ to determine the total pixel area and percent pixel area of each cell marker occupied in granuloma cross sections, as well as co-localization between the macrophage markers and GLUT1. To identify if there is a relationship between glucose uptake and mycobacterial antigens, we performed a glucose uptake assay and hypoxic experiments using 2-NBDG on monocyte-derived macrophages that were stimulated with inactivated Mtb. Image analysis revealed co-localization of different cell markers and GLUT1. When looking at co-localization of CD11c and CD163 with GLUT1, we found that CD11c+CD163- epithelioid

macrophages, the cells in granulomas that are most commonly infected with Mtb, expressed more GLUT1 than interstitial and alveolar macrophages. Moreover, we see evidence that macrophages increase their glucose (2-NBDG) uptake when stimulated with inactivated Mtb. Identifying immune cells that express GLUT1 and what triggers these immune cells to switch to glycolytic metabolism will help us further understand overall granuloma metabolism and cell differentiation after *Mtb* infection. In terms of public health, by better understanding the immunometabolism of granulomas, it will improve monitoring of disease progression or to aid in the treatment of *Mtb* infection to help reduce tuberculosis cases worldwide.

Table of Contents

List of Tables

List of Figures

1.0 Introduction

1.1 Mycobacterium Tuberculosis and TB: Past and Present

Mycobacterium tuberculosis (*Mtb*) belongs to a group of facultatively intracellular bacteria that infect and cause disease in humans (1). These bacteria infect a wide variety of animals including deer, livestock, and badgers (2) and cause granulomatous disease including tuberculosis (TB), the disease most commonly associated with *Mtb* infection. TB is a disease of historic significance and has accounted for a large amount of morbidity and mortality going back to antiquity (3). For example, evidence of spinal TB in ancient Egyptians was found in mummies as far back as 3500 BC (4). In the 17th century, TB, also known as consumption and was widely present in England (5). John Locke, a English philosopher, attributed 20% of all death in London were due to TB (5). TB is not just a disease of the past and it remains a pressing global health concern. It is estimated that a third of the world's population is infected with *Mtb*, with 10 million cases of active TB in 2018 worldwide and more than 1.5 million deaths from TB (6). The largest number of TB cases occur in South-East Asia, Africa, and Western Pacific (7). Moreover, TB is one of the top causes of death among people who are co-infected with HIV (6, 8).

1.2 TB Presentation, Treatment, and Vaccination

Individuals are often described as having latent or active TB based on their symptoms and clinical signs (9). Nearly a third of world is estimated to have latent TB, a state where individuals

are asymptomatically infected with *Mtb*, or at least have anti-*Mtb* responses suggesting they have been exposed to bacterium (9). Importantly, individuals with latent TB cannot transmit the bacterium but can progress to active TB if they become immunosuppressed by cytokine-suppressing drug treatments, HIV infection, or diabetes (10, 11). Individual that have active TB have symptomatic disease and can transmit the bacterium to suspectable people by coughing, sneezing, or spitting into the air (12). About 5-15% of persons infected with *Mtb* will develop active disease and can transmit the disease to another person (13). Symptoms of active disease include cough with sputum and possible blood, chest pains, fever, night sweats, and weight loss (14). Sputum from people with active disease may contain detectable *Mtb (14)*.

A common way to determine *Mtb* infection in latent TB infection is using TB skin test (TST) or a positive interferon-gamma release assay (IGRA) if vaccinated with BCG for TB (15). Unfortunately, neither test can distinguish previous infection, clearance, or risk of disease progression to active disease (15). Laboratory diagnosis of active TB infection can be completed in several ways, such as culture methods that could take weeks to complete or molecular testing techniques provide more rapid diagnoses of TB (16). Culture methods require sputum of an infected patient to be placed into a medium that will promote the growth of the bacterium (16). Sputum can also be stained with Ziehl-Neelsen, fluorescently with auramine or auramine/rhodamine, or using acid-fast staining to stain for *Mtb* (16). Once growth is detected, specie-specific fluorescently-labeled nucleic acid probes can be used to identify the species of the bacterium (16). By using this method, results of the sputum culture will take about 2 weeks (16). Nucleic acid amplification, on the other hand, provides more rapid diagnosis of *Mtb,* including a PCR based method that targets the TB-specific portion or the 16s ribosomal RNA gene with a colorimetric detection system (16). Although PCR based methods are faster, there is a higher false

positives as compared to culture methods (16). Culture methods are the gold standard for confirmation of *Mtb* infection and allow for drug susceptibility testing and genotyping (17). TB can also be diagnosed with PET/CT, a clinical instrument that measures positron emission from a radiolabeled probe. ^{18}F-FDG (fluorine-18 fluorodeoxyglucose) is the PET probe most commonly used for TB diagnosis, and this radiolabeled glucose analog can be used to image lung inflammation (15). Although this method cannot identify the cause of the inflammation, tuberculous granulomas can be detected by PET/CT and changes in PET avidity can be used to identify progression from latent to active TB disease (15).

Treatment of drug sensitive TB requires accurate and early diagnosis, drug resistant screenings, and six months of two phases of drug regimens through directly observed therapy (DOT) (18). The first phase is using a treatment of four drugs, isoniazid, rifampicin, pyrazinamide, and ethambutol (first-line drugs) for two months (18). The next phase is four months using isoniazid plus rifampicin, which is considered a short course chemotherapy (18). Unfortunately, there a cases of multidrug resistance (MDR-TB) and extensively drug-resistant (XDR-TB) that requires more extensive treatment (18). In the case of MDR-TB, treatment is administered for a total of 20-28 months using first-line anti-TB drugs, followed by a combination of 4 second-line anti-TB drugs (para-amino salicyclic acid, streptomycin, ethionamide, ofloxacin, capreomycin, kanamycin, amikacin, or cycloserine) (18). XDR-TB treatment requires the use of third-line anti-TB drugs, such as clofazimine, linezolid, amoxicillin plus clavulanate, imipenem plus cilastatin, or clarithromycin (18).

The only vaccine currently available for TB is based on an attenuated strain of *M. bovis* (19). This vaccine strain, referred to as *M. bovis* bacillus Calmette-Guérin (hereafter referred to as BCG) was developed by using a virulent bovine strain of tubercle bacillus cultured in bile,

glycerin, and potato medium that was then sub-cultured at 3 week intervals (19). Due to WWI, 230 sub-cultures were then carried out and produced a tubercle bacillus that failed to produce progressive TB in several animal models (1919) and in human trials (1921) and was therefore introduced to the public in 1931 (19). Today, there are three different BCG vaccines strains in which the majority of the world's population is supplied (19). BCG's greatest protective benefits are centered on preventing certain presentations including severe disease presentations in children that have military TB and TB meningitis, but it does not prevent pulmonary TB (20). Moreover, BCG's efficacy is highly variable across populations and effectiveness is reduced over time (21). Revaccination does not have protective benefits in adults and the initial BCG vaccination can confound PPD testing for Mtb infection (15, 22). IGRAs remain useful because BCG does not contain the RD1 genomic region encoding the Mtb proteins recognized by IGRAs (15, 23).

1.3 Models of TB Research

There are a wide range of animal models that are available to study Mtb infection. These models include zebra fish, mice, rabbits, cattle, and non-human primates (NHP) (24). Each model has pros and cons in terms of pathology, immunology, and genetics related to tuberculosis in humans (24). For example, mice have diverse genetic and immunologic backgrounds that allow researchers to control specific characteristic such as removing particular genes to determine its relationship to disease progression (24). On the other hand, mice are unable to form granulomas that are phenotypically similar to disease in humans (24). This theme can be seen in every animal model, where some models bring certain characteristics that other models do not. For this thesis, we used granulomas from cynomolgus macaques, a NHP model that is physiologically and

immunologically similar to humans (1, 25). NHP can exhibit a broad range of lesions (or granulomas) that are phenotypically and functionally similar to humans granulomas (24). Additionally, many regents that are used in human immunology can be used on NHP (24). As stated previously, PET/CT with ^{18}F-FDG is commonly used to identify pulmonary inflammation in humans (15). PET/CT can also be used in NHPs to identify inflammation caused by *Mtb* infection (26).

1.4 Mtb Infection Leads to Granuloma Formation

Granuloma formation is the hallmark of TB disease (1, 25). Granulomas can form in any tissue that becomes infected with *Mtb* but because *Mtb* is transmitted via aerosol route and the lung is the primary site of infection, granulomas are most commonly found in lung tissue (1). Once inhaled, *Mtb* are phagocytosed by alveolar macrophages in the respiratory tract (27). Although macrophages are normally good at killing bacteria, *Mtb* are evolved to stop the phagosomal maturation and macrophages are their preferred host cell (28). Once inside a macrophage, *Mtb* replicate until they lyse the cell, and in the lungs, this recruits other phagocytes including interstitial macrophages and neutrophils that can be subsequently infected and serve as new host cells (1, 29). This process is repeated until antigen or bacteria-containing dendritic cells migrate to lymph nodes and prime adaptive immune response against *Mtb* and T cells are recruited to the site of infection (30). The early stages of granuloma formation are not well understood, but in cynomolgus macaques, a nonhuman primate where *Mtb* infection leads to human-like TB disease (31), necrotic granulomas that have lymphocyte cuffs, well-differentiated macrophage regions, and necrotic centers are already formed by four weeks post infection (32). This timeframe also

coincides with the ability to detect granulomas by PET-CT (26). There are many types of granulomas, including necrotic (caseous) granuloma, which is the most common lesion for active TB (32). Other types include nonnecrotic, cellular, fibrocalcific, and suppurative granulomas (32). Although necrotic (caseous) granulomas are seen more in active TB, it can be present in latent TB as well (33).

1.5 Granuloma Macrophages are Phenotypically and Functionally Diverse

Macrophages are major constituents of the cells that make up a granuloma and are found throughout these lesions but are especially abundant in the macrophage region (32). Macrophages in this region undergo distinct morphological changes and are referred to as epithelioid macrophages (25). Macrophages in the different granuloma regions are phenotypically different and CD11c and CD163 expression can be used to differentiate alveolar macrophages, lymphocyte cuff, and epithelioid macrophages (32). Alveolar macrophages are strongly CD11c+CD163+, while CD11c+CD163- macrophages (epithelioid) are seen in the macrophage region and CD11c-CD163+ macrophages (interstitial) are seen in the lymphocyte cuff (32).

Macrophage functions are often differentiated by the metabolic pathways they use for arginine catabolism (34, 35). Both M1 and M2 macrophages utilize arginine but (25) M1 macrophages catabolize arginine via inducible nitric oxide synthase (iNOS) to produce the antibacterial gas nitric oxide whereas M2 macrophages use arginase 1 (Arg-1) to generate polyamines (25, 35). In mice, these functional states are often categorized into two different functional states (M1 and M2 polarized macrophages) where M1 macrophages have pro-inflammatory and microbicidal functions driven by Th1 T cell cytokines including TNF*y* and IFNg

and M2 macrophages have anti-inflammatory pro-healing functions driven by Th2 cytokines including IL-4 (34, 36). Granuloma macrophages also express these enzymes and while the differences between M1 and M2 macrophage are not as distinct in primates as in mice, granuloma macrophages exhibit distinct functional states (32). Moreover, iNOS and Arg-1 expression were region specific with iNOS more strongly expressed in the macrophage region than the lymphocyte cuff, while the iNOS:Arg-1 ratio of these regions suggesting the epithelioid macrophages are more M1-like than lymphocyte cuff macrophages (32).

1.6 M1 and M2 Macrophages Use Different Routes to Generate ATP

Immune cells, such as macrophages, use different metabolic pathways including oxidative phosphorylation and glycolysis to generate ATP under different conditions (1, 25). Glycolysis generates 2 molecules of ATP and oxidative phosphorylation generates 36 ATP from 1 molecule of glucose (37). Oxidative phosphorylation ultimately produces more ATP than glycolysis, but glycolysis produces ATP faster and provides metabolic intermediates that are needed for cell growth and proliferation (1). More so, enhanced glycolysis enables immune cells to generate biosynthetic intermediates to carry out effector functions such as phagocytosis and inflammatory cytokine production in macrophages (37).

M1 and M2 macrophages differ in immune-metabolic response in the presence of *Mtb* (25). M1 macrophage polarization is characterized by an up-regulation of genes consistent with the Warburg effect (25). The Warburg effect is a phenomenon where cells switch their metabolic profile to utilize glycolysis to generate ATP even in the presence of oxygen, also referred to as aerobic glycolysis (25, 38). After stimulation with LPS or TLR ligation, M1 macrophages increase

hypoxia-inducible factor 1-α (HIF1α), expression associated with the Warburg effect (25, 39, 40). Overexpression of HIF1α will suppress mitochondrial oxidative phosphorylation (41, 42). Unlike M1 macrophages, M2 macrophages upregulates Arg-1, signal transducer and activator of transcription 6 (STAT6), and GATA binding protein 3 (GATA3) in order to produce anti-inflammatory cytokine IL-10 (25). M2 macrophages have an intact TCA cycle to allow for the generation of ATP through oxidative phosphorylation and concomitantly display increased glycolysis as a carbon source (43, 44). Enhanced utilization of glycolysis occurs in other immune cells including dendritic cells (DCs), natural killer cells (NK), and T cells where it is important for rapid replication and high levels of activity including cytokine expression (37). Glycolysis is also important for tumor cells and enables them to survive and replicate rapidly in normoxic and hypoxic environments (38).

The first step in glycolysis is transportation of glucose across the plasma membrane (45). Transport of glucose across the cell membrane is mediated by facilitative glucose transporter proteins (GLUTs), and there have been fourteen GLUTs identified so far (45). Each GLUT differs in their tissue distribution and affinity for glucose, but GLUT1 is expressed broadly throughout the body and heavily studied in cancer because it is elevated expression in almost all human cancers (45). GLUT1 is a well characterized glucose transporter expressed by leukocytes that has been used as an indicator of immune cell glycolysis metabolism (37). GLUT1 contains 492 residues, containing N and C domains that take in substrate, such as glucose, into the cell (46). Substrate binding on the C domain induces the closure of the N and C domains on the extracellular side (46). As affinity for the intracellular side increases after substrate binding on the extracellular side, this causes GLUT1 to change to an open-conformation structure and allow substrate dissociation (46).

The metabolic interactions between immune cells in granulomas are not fully understood but may improve therapies that reduce the duration of TB treatment. This approach is currently being investigated for cancer, where targeting glycolysis is being explored as a tool for cancer treatment, either as an approach that directly targets tumor cells or enhances the activity of chemotherapeutic agents (47). Before this approach can be considered in TB, several aspects of granuloma biology need to be investigated to assess its feasibility. Moreover, PET-CT using 2-fluoro-2-deoxy-D-glucose (^{18}F-FDG), a glucose analog, has become an increasingly important tool for diagnosing TB (48). ^{18}F-FDG accumulates in cells through glucose transporters (GLUT) and can be visualized by PET (49). Uncovering the drivers of glucose uptake, as visualized by ^{18}F-FDG PET, can be translated into meaningful insight into cellular changes in granulomas. In addition to ^{18}F-FDG, studies have shown that 2-NBDG, a fluorescent analog of D-glucose, can also be used to as a probe for monitoring glucose uptake in malignant tumor cells (50).

For my thesis, we used GLUT1 expression as a proxy for glycolytic metabolism in granulomas. Moreover, we used 2-NBDG in experiments with monocyte-derived macrophages to identify the relationship between *Mtb* antigens and macrophage glucose uptake, thus offering mechanistic insights into granuloma biology. The hypothesis addressed here is that macrophages from lung granulomas in regions of hypoxia or after exposure to *Mtb* antigens will express more GLUT1 as compared to regions of normoxic conditions or lower *Mtb* exposure. Thus, the specific aims are to (1) identify which cell types in granulomas use glycolysis as their energy source; and (2) identify potential drivers of glycolysis in granuloma macrophages. **Figure 1** shows the workflow we used to test my hypotheses. I expect that a deeper understanding of immunometabolism in granulomas may lead to better diagnostics and therapeutics for this globally-significant disease.

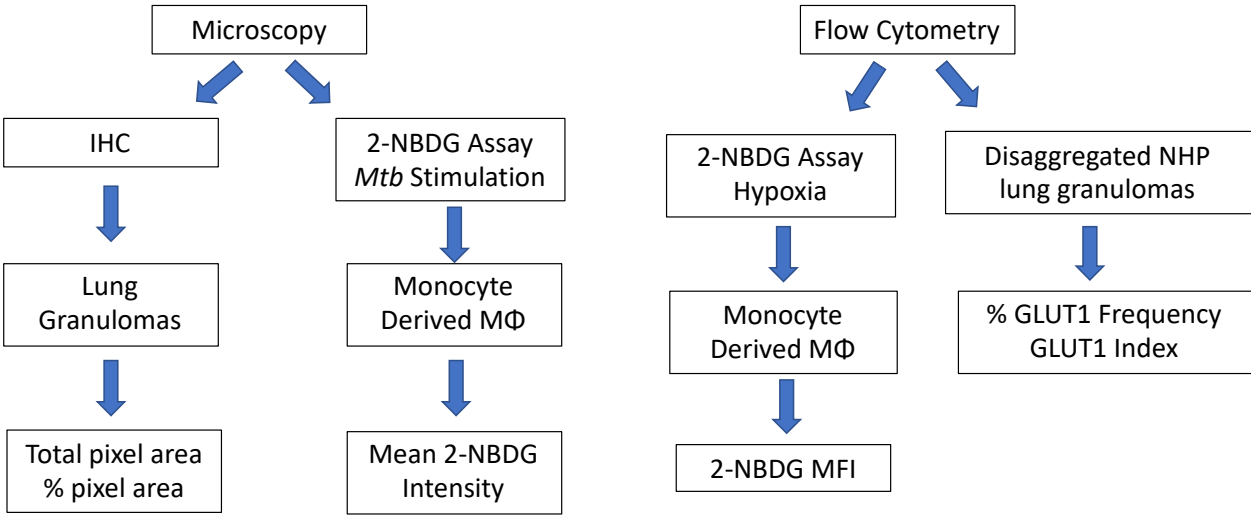

Figure 1. Workflow of Thesis Project

2.0 Methods and Materials

We used GLUT1 expression as a proxy for glycolysis in granulomas. We hypothesized that macrophages may express significant levels of GLUT1 because previous work has shown that the macrophage region can be hypoxic (51) and these cells may need to use glycolysis to survive in this environment. To identify where GLUT1 is expressed and if granuloma macrophages use glycolysis as their energy source, slides with lung granulomas from *Mtb*-infected NHPs were obtained for immunohistochemistry (IHC). IHC allows for the staining of specific cell markers for different macrophage subsets and GLUT1. Then, these granulomas were imaged with a Nikon e1000 microscope to visualize GLUT1 expression and macrophages subsets. IHC is limited by the number of colors that can be visualized by our microscope, the different antibody host species that can be combined in one cocktail, and the different staining patterns of the cells can present a problem with analysis. In order to determine if other cells (T cells, B cells, neutrophils, and CD3-CD20- lymphocyte-sized cells) express GLUT1 in granulomas, we stained single cell suspensions from NHP granulomas and measured their GLUT1 expression by flow cytometry.

To address my second aim of identifying potential drivers of glycolysis in granulomas, we used a glucose uptake assay using 2-NBDG, a fluorescent glucose analog where we stimulated monocyte-derived macrophages with gamma-radiated *Mtb* (*yMtb*). We also performed these experiments under hypoxic conditions to determine if these macrophages take up 2-NBDG in an environment with limited oxygen. We also measured if stimulation with *yMtb* changed 2-NBDG uptake.

2.1 GLUT1 Expression in Macrophage Subsets in Lung Granulomas

In order to conduct studies for my first specific aim (determining which cell subsets express GLUT1 within a granuloma), 23 slides with NHP lung granulomas were obtained. From these slides, we identified 33 granulomas from nine NHP (**Table 1**). We stain these slides by IHC using antibodies specific for cell markers including the macrophage markers CD11c and CD163, and glucose transporter GLUT1. We imaged these slides with a Nikon e1000 microscope to visualize macrophage and GLUT1 localization. We then used ImageJ to determine the total area (pixels) and percent area (pixels) each macrophage marker and GLUT1 staining.

Table 1. Slides of Lung Tissue Granuloma Stained with GLUT1 CD11c CD163

NHP #	Sample #	Tissue Type	Granuloma Type	ROI Area (pixels)
M3609	12A1	LLL Medial/LLL cluster	Coalescing caseous	51,526,122
M3609	12A2	LLL Medial/LLL cluster	Coalescing caseous	27,678,810
M3609	12A3	LLL Medial/LLL cluster	Coalescing caseous	50,753,910
M6409	8	RLL Cluster B/RLL GR4	Coalescing caseous	14,662,496
M6410	6A	RUL granl	Interstitial scar/mineralization	17,751,200
M6410	6B	RUL granl	Interstitial scar/mineralization	17,034,368
M6410	21	RLL granl 7B	Necrotizing	12,462,606
M6810	4	RUL GR 1	Necrotizing caseous	17,717,380
M6810	21	RLL GR 6	Coalescing necrotizing (caseous)	22,115,904
M6810	24	RLL GR 9	Necrotizing caseous	19,657,524
M7110	8	RLL GR 1	Coalescing necrotizing (fibrinoid) alveoltis	8,341,952

Table 1 Continued

M7110	10	RLL 3 GR	Necrotizing with fibrinoid (early caseous)	34,178,364
M11208	26	RLL GR 6	Caseous (mineralization/fibrosis)	44,720,068
M12603	9A	Lung GR	Unspecified	15,785,324
M12603	9B	Lung GR	Unspecified	52,718,262
M18314	40A1	RML 10 area	Coalescing necrotizing (caseous)	9,872,118
M18314	40A2	RML 10 area	Coalescing necrotizing (caseous)	12,520,848
M18314	40A3	RML 10 area	Coalescing necrotizing (caseous)	7,262,667
M18314	40B1	RML 10 area	Coalescing necrotizing (caseous)	22,354,392
M18314	40B2	RML 10 area	Coalescing necrotizing (caseous)	25,489,984
M18314	40B3	RML 10 area	Coalescing necrotizing (caseous)	12,527,352
M18314	40C1	RML 10 area	Coalescing necrotizing (caseous)	12,988,032
M18314	40C2	RML 10 area	Coalescing necrotizing (caseous)	10,270,916
M18314	48A	Access with granl	Necrotizing and non-necrotizing with possible fibrous	7,763,080
M18314	48B	Access with granl	Necrotizing and non-necrotizing with possible fibrous	34,872,848
M18314	48C1	Access with granl	Necrotizing and non-necrotizing with possible fibrous	10,439,048
M18314	48C2	Access with granl	Necrotizing and non-necrotizing with possible fibrous	12,551,070
M18314	48C3	Access with granl	Necrotizing and non-necrotizing with possible fibrous	4,208,268
M21310	8	LLL cluster 8 GR	Coalescing necrotizing with TB pneumonia	117,079,044
M21310	23	Access granl 5	Coalescence non-necrotizing with fibrous	8,864,456
M21310	29	LLL granl 4	Necrotizing (caseous) and non-necrotizing	18,059,424
M21310	44	LUL granl 1	Fibrous necrotizing (caseous) and non-necrotizing	37,942,288

2.2 Immunohistochemistry

Antigen retrieval was performed as previously indicated (32, 52). The slides were deparaffinized by incubating them twice in xylene and then twice in 95% ethanol for five minutes each. The slides were then placed into antigen retrieval buffer and placed into a pressure cooker. After the pressure cooker ran its cycle, about 45 minutes, the slides were rinsed with PBS. Each slide contained two serial sections of tissue. One section was designated to be stained with antibodies against the markers of interest and the other served as a no-primary control for nonspecific binding. Both sections were blocked with 2% BSA-PBS for 30 minutes. The primary cocktail included antibodies against GLUT1, CD11c, and CD163. CD11c and CD163 are macrophage markers and can be used in different combinations to identify different macrophage where CD11c+CD163- cells are epithelioid macrophages, CD11c-CD163+ cells are interstitial macrophages, and CD11c+CD163+ cells are alveolar macrophages (32). The GLUT1 (polyclonal, dilution 1:30; Thermo Fisher Scientific), CD11c (clone 5D11, dilution 1:30; Leica Microsystems, Buffalo Grove, IL), and the CD163 (clone 10D6, dilution 1:50; Lab Vision). After 30 minutes, the blocking buffer was removed, and the primary antibody cocktail was added to the tissue section designated for antibody staining and blocking buffer was added to the no-primary control tissue section and incubated for one hour. During this time, a cocktail of fluorophore-conjugated secondary antibodies specific to the primary antibody was made. The secondary antibodies for GLUT1, CD11c, and CD163 were AlexaFluora (AF) 594 anti-rabbit IgG, AF647 anti-mouse IgG2a, and AF488 anti-mouse IgG1, respectively. Once the one-hour incubation for the primary stains was complete, the slides were washed three times in 1X phosphate buffered saline (PBS), three times. Mounting media with DAPI, which stains nucleated cells, was used to adhere a coverslip to the slides.

2.3 Microscopy

Fluorescent microcopy was performed on a Nikon e1000 epifluorescence microscope operated by the Nikon NIS Elements software. Fluorescent microscopy uses excitation light that lets through radiation with a certain wavelength that is specific to the fluorophore that is attached to the sample of interest (53). This causes the electrons associated with the sample to be excited to a higher energy level and then relaxed to a lower level and emit light (53). Through different filters within the microscope, it is able to separate out much brighter excitation light from the lower energy emitted light to be viewed by the human eye (53). By using this microscopy technique, we could visualize GLUT1 expression and identify which macrophage subsets express GLUT1 within a lung granuloma. The microscope we used can image four channels including the wavelengths that excite DAPI (visualized as white), AF488 (green), AF594 (red), and AF647 (far-red; pseudocolored blue). To make our image analysis quantitative, the camera region of interest used for image acquisition, and camera exposure settings were consistent among all slides. All images were taken a with a 20x magnification with a non-oil immersion Nikon Plan APO lens.

The image lookup tables (LUTs) were adjusted according to the no-stain control to minimize the autofluorescence and background for each fluorophore and the same set of LUTS was applied to all the images within a set. Each animal's tissue has a different autofluorescence and background profile and the LUT table for each animal was adjusted independently. Images were acquired as four channel ND2 files and then converted into two TIFF files, one with only the DAPI channel, and the other with only the RBG (red-TRITC, pseudocolored blue-Cy5, and green-FITC) channels. Some pieces of tissue were too large to be imaged in a single stitched field and needed to be imaged with several overlapping fields to get the whole tissue section of interest.

These photos were exported as TIFF files and merged together using Adobe Photoshop's Photomerge feature and analyzed with ImageJ.

2.4 Image Analysis with ImageJ

Beth Junecko made a macro for ImageJ that allowed us to determine the total area and percent area in pixels of each marker of interest (**Appendix 1**). First, the macro requires the TIFF DAPI image to create a region of interest (ROI). By selecting an ROI, we were able to isolate specific granulomas within the image and remove any adjacent lung or tissue that is not involved in the granuloma. After the ROI is created, the macro requires the TIFF RBG image and applied the ROI to that image. From here, the macro splits the TIFF RBG image individual images for each channel (red (TRITC), blue, and green). The macro then goes through each channel and allows the user to adjust the threshold. By adjusting the threshold up or down, the user determines which pixel are foreground and background by choosing a value cutoff. Every pixel less than that value cutoff is considered in the foreground and every pixel more than that value is considered the background. For example, if the threshold is adjusted to 0, then no pixel is accounted for and if the threshold is adjusted to the max (255), then all pixels are accounted for within the image for that specific channel. But adjusting the threshold between 0 and 255, the user determines which pixels within that image are actually positive for that channel. Once the threshold is determined by the user, the macro will repeat this process for each channel and DAPI. Once the thresholds are determined for each channel and DAPI, the macro can then determine the total pixel area and percent pixel area for each channel and any co-localization of multiple channels together. For our macrophage markers, we looked at the overall expression of GLUT1, CD11c, and CD163 within

each granuloma. We also determine which macrophages expressed GLUT1 and CD11c only (epitheliolid), GLUT1 and CD163 only (interstitial), and GLUT1, CD11c and CD163 (alveolar) together. This allows us to determine which subsets of macrophages that were and were not expressing GLUT1. Additionally, we can see that there are cells that were not positive for our macrophage markers but expressed GLUT1.

Each slide that was stained and analyzed to determine if there were multiple granulomas per slide (**Table 1**). In some cases, an individual block may contain multiple pieces of tissue and we have given letters to designate each tissue in these instances. Tissues with multiple granulomas were given a number along with the letter, for example, M18314 (40) had several pieces of tissue labeled as 40A, 40B, and 40C and these pieces contained several granulomas labeled as 40A1, 40A2, 40A3, and so on. Lack of a letter and number designates that slide had one piece of tissue with one granuloma within that tissue.

The type of granulomas we examined and size (number of pixels in each image) for each granuloma are indicated in **Table 1**. Granulomas come in several different phenotypes including fibrotic and mineralized granulomas and non-granulomatous lung contains structures that strongly express GLUT1 including ciliated epithelium. We focused on necrotic and non-necrotic granulomas because these granulomas are most similar to each other in terms of their cell types (and because the mineralized and fibrotic granulomas in our sample set were often damaged during sectioning) we selected ROIs that excluded fibrotic and mineralized granulomas, ciliated epithelia, and red blood cells (which also express significant amounts of GLUT1) for our analysis.

The total area and percent area of pixels was determined for each color combination where each combination represents a cell population and GLUT1 expression state. Additionally, the number of cells within the granuloma by using DAPI was used to get a count for the number of

cells within each granuloma, since it stains the nucleus of each cell. Although we tried to quantify the number of macrophages per section, the morphology of these cells and the way they cluster together prevented us from quantifying them as individual cells and we used pixel areas occupied by the macrophage markers instead.

2.5 Flow Cytometric Analysis of GLUT1 Expression

We applied a similar approach to assess GLUT1 expression by neutrophils and T cells by staining for calprotectin, a protein that is abundant in the cytoplasm of neutrophils, and CD3, respectively. While our staining worked, we found that the different staining patterns (cytoplasmic for neutrophils and cell surface for T cell) for the cell types and low signal:background ratio for the T cells limited our confidence in these results. To address this question, we stained cells from NHP granulomas and assessed them by flow cytometry. This work was performed under BSL3 conditions by Josh Mattila and Beth Junecko and I contributed to data analysis. We obtained granulomas from three NHP that were included as untreated controls (n=3) in an ongoing study (23 total granulomas) (**Table 2**).

Table 2. Homogenized lung granulomas from NHP used in flow cytometry analysis of GLUT1 expression in T cells, B cells, and myeloid cells

NHP #	Granuloma # and Tissue Type
22018:	A- RLL 1 B- LLL 7 C- LLL 9 D- LLL 4 E- LLL 5 F- RLL 3 G- RLL 10 H- RLL 11 I- RLL 2
23318:	A- LLLgr3 B - LLLgr1 C - LLLgr2 D - RLLgr4 E - RLLgr3 F - RLLgr2 G- RLLgr1
23818:	A - LLL 1 B - RLL 1 C - RLL 3 D - RLL 4 E - RLL 2 F - RLL 6 G - LLL 4

These granulomas were homogenized with Miltenyi gentleMACS tissue dissociators using the enzymes included in the human tumor dissociation kit. The single cell suspensions were stained with fluorochrome-conjugated antibodies against CD3 (T cells), CD20 (B cells), and the myeloid markers CD11b, CD11c, CD14, CD206, and GLUT1. After 20 minutes of incubation at room temperature, the cells were washed and fixed, transferred out of the BSL3 and intracellularly stained for calprotectin using the BD Cytofix/Cytoperm kit. Stained cells were run by Josh Mattila

on the BD LSRFortessa flow cytometer maintained by the Department of Infectious Diseases and Microbiology. Analysis was done with FlowJo using anticipated antigen expression profiles for each cell population under the gating strategy. For the purpose of the thesis, only animals that were left untreated (n=3) were used to analyze GLUT1 expression in T cells, B cells, and myeloid cells.

2.6 Experiments with 2-NBDG

We used a fluorescent glucose analog, 2-NBDG (2-[*N*-(7-nitrobenz-2-oxa-1,3-diazol-4-yl)amino]-2-deoxyglucose) (**Appendix 2**), and *Mtb*-stimulated monocyte derived macrophages as a model for granuloma macrophages to determine if bacterial antigens can induce glucose uptake in granulomas. We also performed these experiments under hypoxic conditions in a desiccator where the oxygen had been removed by burning a candle to determine if hypoxia also contributed to glucose uptake.

2.7 Glucose Uptake Assay

Monocytes were isolated from Percoll gradient-isolated PBMCs with Miltenyi anti-human CD14 magnetic beads and cultured in macrophage media made up of RPMI and 10% FBS (R10) in 12-well plates for 7-10 days. Then the cells were lifted off and reseeded onto 12-well chamber slides (about 50,000 cells/well) from four different NHPs (M22618, M13618, M21718, and M22118). To prepare the 2-NBDG from packaging, 5mg of the 2-NBDG was dissolved in 500uL of 100% ETOH (10mg/mL). A 1:4 mixture of 2-NBDG:PBS was made and 10 microliters of this

mixture was added to each well with no gamma-radiated *Mtb* (*yMtb)* and 2-NBDG only, as shown in **Table 3**. With the remainder of the 2-NBDG:PBS mixture, 5 microliters of *yMtb* was added. The wells that were designated to receive stimulation of *yMtb*, received 11 microliters of the *yMtb*-2-NBDG:PBS mixture. At each timepoint, 100 microliters of the media from each duplicate well was removed and 200 microliters of 2% PFA was added to stop the reaction. Once all time points were completed, all media was removed, and the wells were washed with 1xPBS twice. The chamber was removed from the slide and Prolong Gold mounting media with DAPI was used to adhere a coverslip to the slide. For cells on slides, images were acquired of each well with a Nikon e1000 microscope and analyzed with a CellProfiler pipeline created by Josh Mattila to quantify macrophage 2-NBDG uptake by *Mtb* stimulated or unstimulated macrophages at different time-points.

Table 3. Conditions of Monocyte-Derived Macrophages in a 12-well Chamber Slide used in the Glucose Uptake Assay with 2-NBDG

0 Hour	10 Minutes	30 Minutes	1 Hour	3 Hours	Overnight
yMtb- 2-NBDG-	yMtb+ 2-NBDG+	yMtb+ 2-NBDG+	yMtb+ 2-NBDG+	yMtb+ 2-NBDG+	yMtb+ 2-NBDG+
yMtb- 2-NBDG+	yMtb- 2-NBDG+	yMtb- 2-NBDG+	yMtb- 2-NBDG+	yMtb- 2-NBDG+	yMtb- 2-NBDG+

2.8 Hypoxia Experiments

To determine if hypoxia could be a driver of glycolysis in immune cells, we performed a pilot experiment using monocyte derived macrophages from one Mtb-infected NHP (M32419)

where the cells were incubated in FACs tubes instead of on slides. These tubes either received no stimulation, 2-NBDG, *yMtb*, or 2-NBDG with gamma-radiated Mtb and were held in either an oxygenated "normal" environment or an oxygen-lacking hypoxic environment created in a desiccator where a candle had been burned. Cells in oxygenated conditions were put in a 37°C incubator. After 1 hour and 3 hours, the cells were stained for CD3, CD11b and a live/dead indicator stain. These cells were then washed with PBS and fixed using 2% PFA. These cells were then assayed by flow cytometry and analyzed using FlowJo to determine the frequency of cells that are positive for the cell markers and 2-NBDG.

3.0 Results

3.1 GLUT1 Expression in Different Cell Populations in Lung Granulomas

We used 23 slides from several different non-human primates (NHP) that were infected with *Mtb* and identified 33 granulomas in these tissues for analysis. We used immunohistochemistry (IHC) to stain the slides with antibodies against macrophages and GLUT1 and then we used microscopy to image these sections. Our stains include GLUT1, CD11c, and CD163. GLUT1 is stains for glucose transporter 1, CD11c and CD163 are both markers for macrophages (**Figure 2**).

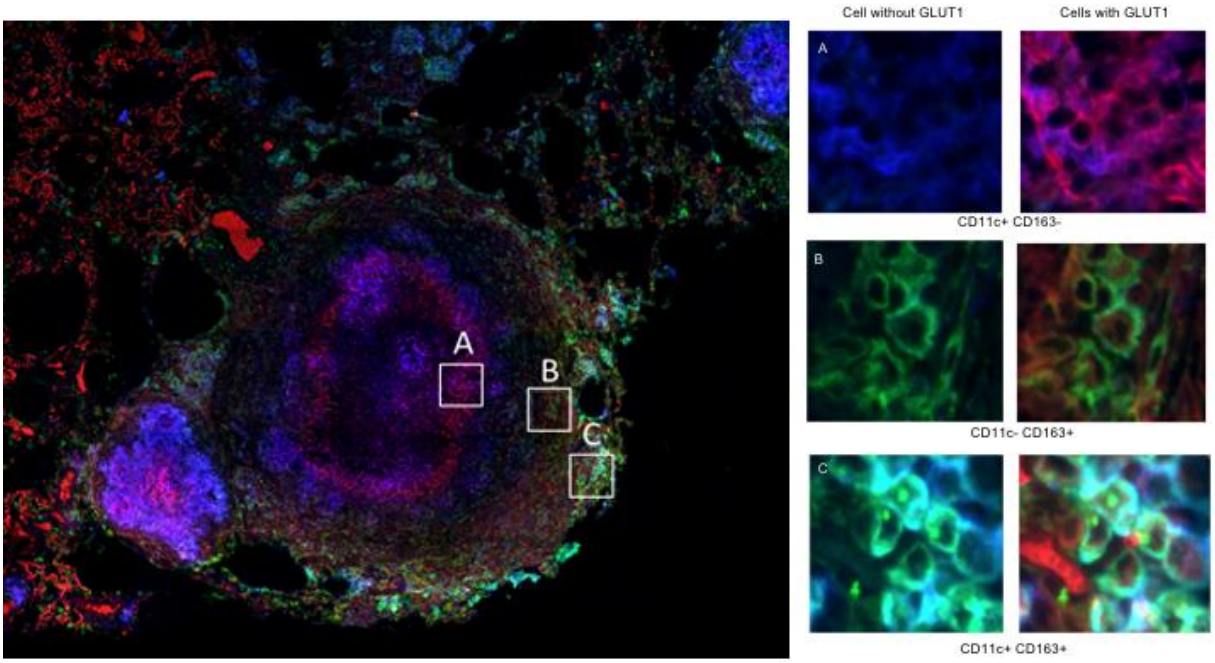

Figure 2. Macrophage subsets in granulomas express GLUT1

Red is GLUT1, blue is CD11c, and green is CD163.

Using ImageJ, we determined the total pixel area and percent pixel area of each stain in each granuloma to analyze GLUT1 expression by epithelioid, interstitial, and alveolar macrophages (**Figure 3**).

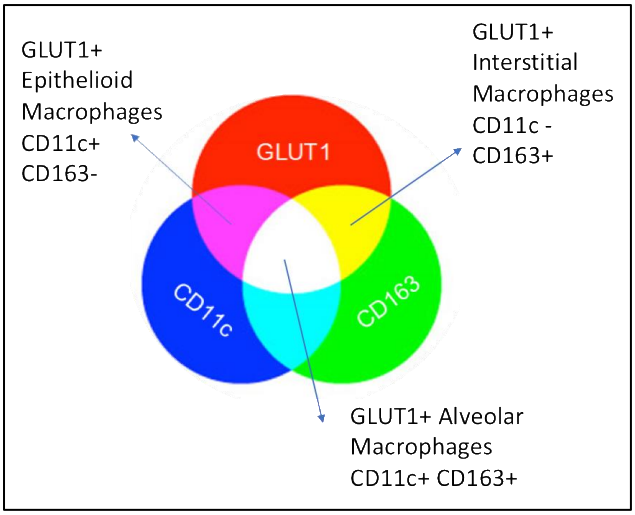

Figure 3. Illustration of how each cell marker was analyzed individually and in colocalization with other cell makers to determine GLUT1 expression of macrophages in lung tissue granulomas

3.2 GLUT1 Expression in Macrophage Subsets

To determine if there was a difference between GLUT1- and GLUT1+ macrophages for each subset, we performed a pairwise comparisons between subsets and used the Wilcoxon test which is a non-parametric test for paired groups to determine if these results were statistically significant. Based on this approach we found that for each macrophage subset, there was significantly more area occupied by GLUT1+ macrophages than area occupied by GLUT1- macrophages in granulomas (**Figure 4**).

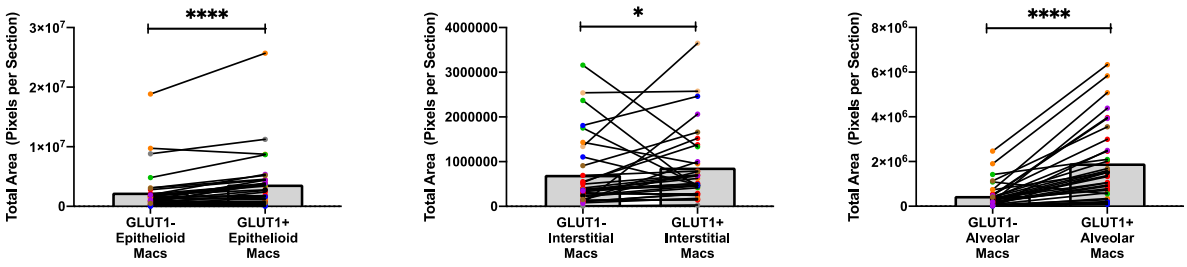

Figure 4. GLUT1+ macrophages occupy more area than GLUT1- macrophages in granulomas

Comparisons of the total pixel area of GLUT1+ to GLUT1- epithelioid, interstitial, and alveolar macrophage subsets.

The granulomas we imaged were of substantially different size profiles and to normalize the differences in size with respect to the granuloma area occupied by each macrophage subset, we also did pairwise comparisons (Wilcoxon test) testing the percent of the granuloma occupied by a macrophage subset (**Figure 5**). Similar to our previous result based on the area occupied by each macrophage subset, we found a significantly higher proportion of the granuloma area was occupied by GLUT1+ macrophages than GLUT1- macrophages.

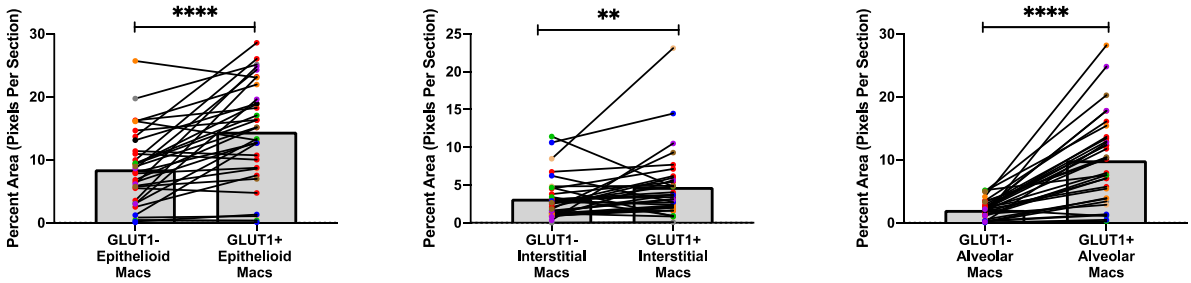

Figure 5. GLUT1+ macrophages occupy a higher proportion of the granuloma's area than GLUT1- macrophages

Comparisons of the percent pixel area of GLUT1+ to GLUT1- epithelioid, interstitial, and alveolar macrophage subsets.

We then wanted to find out how much epithelioid, interstitial, and alveolar macrophages contributed to the overall GLUT1 expression in lung granulomas. Using a non-parametric one-

way ANOVA (Friedman test) to allow multiple comparisons, we compared the total pixel area of the overall GLUT1 expression (total GLUT1+ pixels/ROI) in each granuloma to the GLUT1+ epithelioid, interstitial, and alveolar macrophage subsets. We found that there was a significant difference for each macrophage subset and the overall GLUT1 expression (**Figure 6**). We then summed the GLUT1 expression of all macrophage subsets (epithelioid, interstitial, and alveolar) and compared that to the overall GLUT1 expression. We found a significant difference in the total pixel area between the summed GLUT1 expression of macrophage subsets and the overall GLUT1 expression in lung granulomas (**Figure 6**).

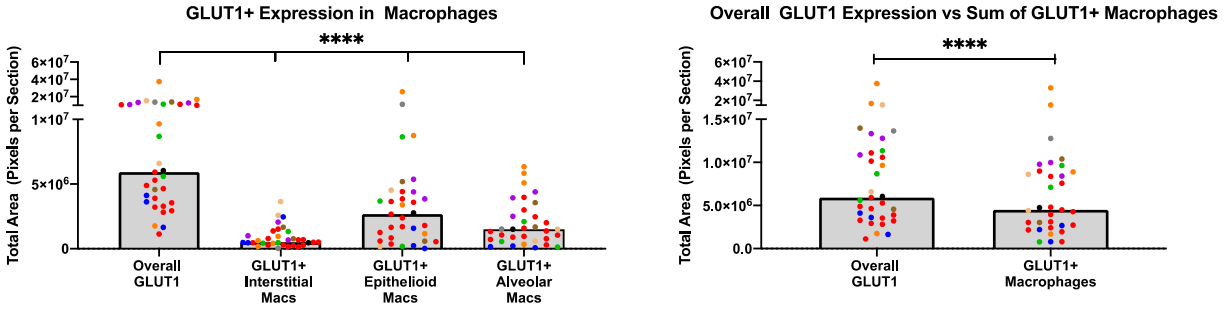

Figure 6. Macrophage GLUT1 contributes to, but is not the only source, of granuloma GLUT1 expression

Comparison of the total pixel area of the GLUT1 expression in each macrophage subset and the sum of all GLUT1+ macrophages to the overall GLUT1 expression in lung granulomas.

To normalize the difference in size of each granuloma, we also made these comparisons using the Friedman test but with the percent pixel area and found the same trend (**Figure 7**) indicating that in macrophages are not the only cell population that contributes to GLUT1 expression in lung granulomas.

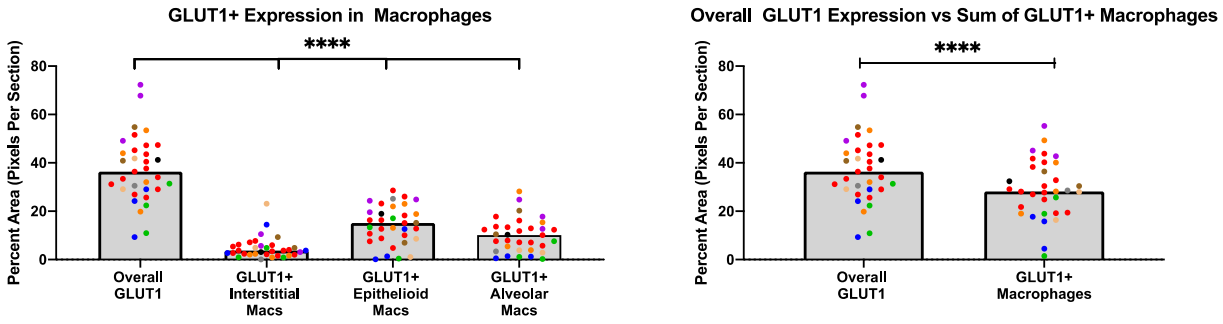

Figure 7. Macrophage GLUT1, when normalized for granuloma area, partially contributes to overall granuloma GLUT1 expression

Comparison of the percent pixel area of the GLUT1 expression in each macrophage subset and the sum of all GLUT1+ macrophages to the overall GLUT1 expression in lung granulomas.

Since the above analysis treats each granuloma from each NHP individually, we decided to look at the data differently by finding the mean total pixel area and percent pixel area among all granulomas for each NHP. Although each granuloma is independent from other granulomas within a host, the response by the host can differ among different hosts. By grouping all granulomas for each NHP and determining the mean, it allows our results to be reproducible and more general among NHP. **Figure 8** compares mean total pixel area and percent pixel area of the overall GLUT1 expression to our GLUT1+ macrophages subsets in among NHP. We found a lack of significant difference between the overall GLUT1 expression and GLUT1+ epithelioid macrophages.

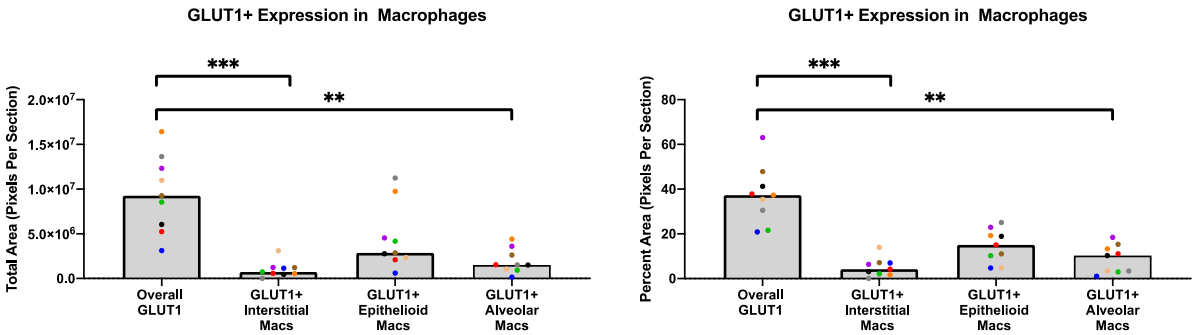

Figure 8. Macrophages contribute to, but are not the sole source, of overall granuloma GLUT1 expression

Comparison of the A) the total pixel area and B) percent pixel area of the GLUT1 expression in each macrophage subset and the to the overall GLUT1 expression in lung granulomas.

3.3 Flow Cytometry with GLUT1

In order to identify the non-macrophage cell types that contribute to overall GLUT1 expression in granulomas, we used flow cytometry to identify GLUT1+ immune cells in lung granulomas. We stained the homogenate for myeloid cells, CD3+ T cells and CD20+ B cells, and also examined the population of unclassified CD3-C20- lymphocyte sized cells. We identified each cell population using the gating strategy shown in **Figure 9**. We calculated the frequency of GLUT1+ cells and the GLUT1 index of B cells, T cells, neutrophils (PMN), macrophages, and unclassified cells by multiplying the number of GLUT1+ cells to the GLUT1 MFI. We used this metric (GLUT1 index), which accounts for the total number of cells in each cell population and GLUT1 expressed by each cell, as a metric of that population's overall GLUT1 signature within a granuloma.

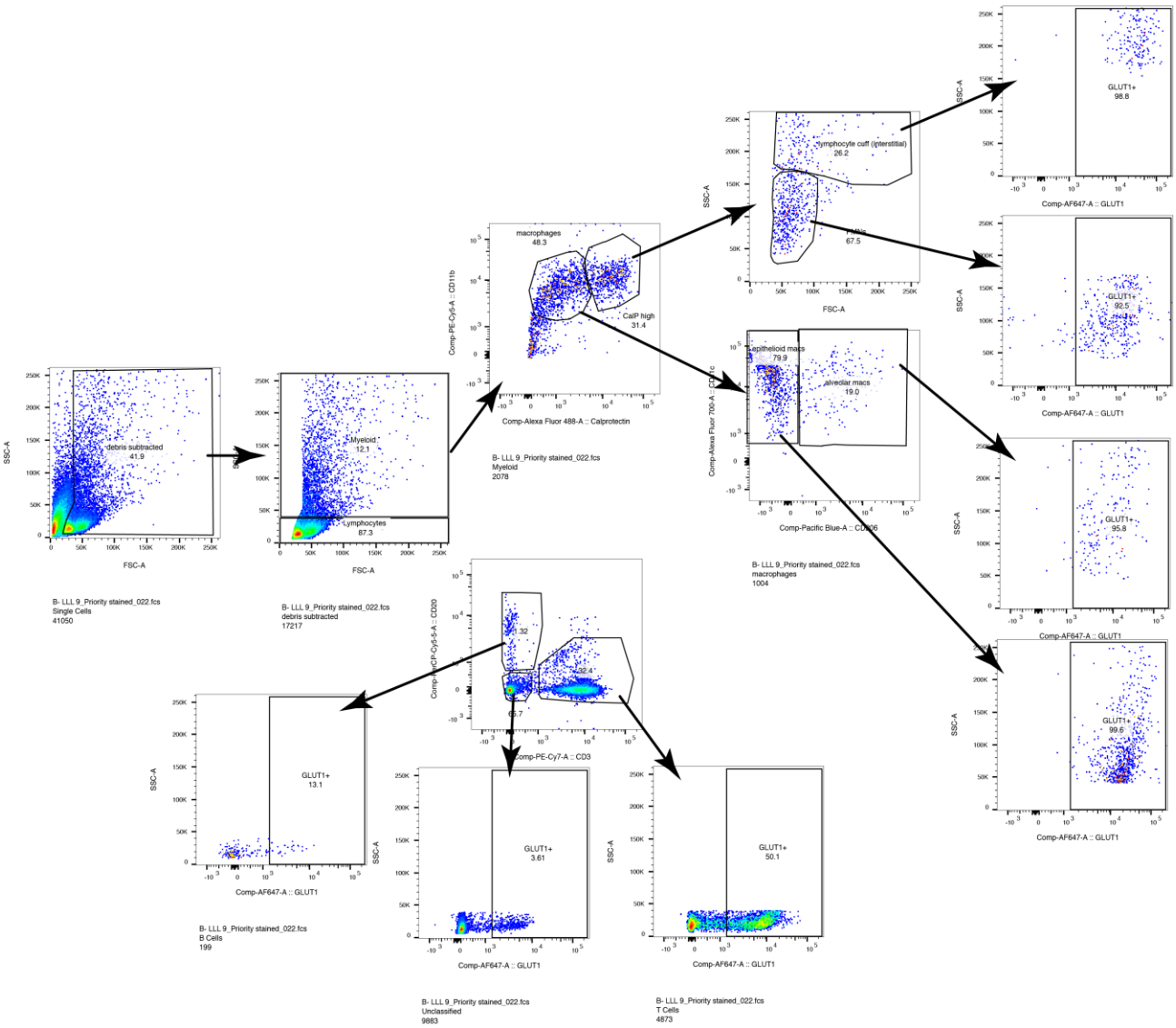

Figure 9. Gating strategy used to isolate T cells, B cells, and myeloid cells from homogenized lung granulomas from macaque granulomas

We first sought to identify the frequency of GLUT1+ cells for each of our gated cell populations (Figure 10 Left) where the individual granulomas are represented by the small dots (red, M22018; grey, M23818; blue, M23318) and the large dots represent the median frequency of GLUT1+ positive for each animal. We are presenting the data in this manner because although granulomas are analyzed as discrete units (the granuloma), an animal will have multiple

granulomas that all have related features that are more similar to each other than to granulomas from another animal. In this regard, each granuloma resembles a replicate in an experiment and the animals represent an independent experiment. For our analysis, we are comparing the individual animal (large dot) data rather than the individual granuloma (small dot) data. Using the Friedman test (non-parametric one-way ANOVA for paired data), we found a significant difference in the frequency of %GLUT1 positive epithelioid macrophages and unclassified lymphocyte-sized cells.

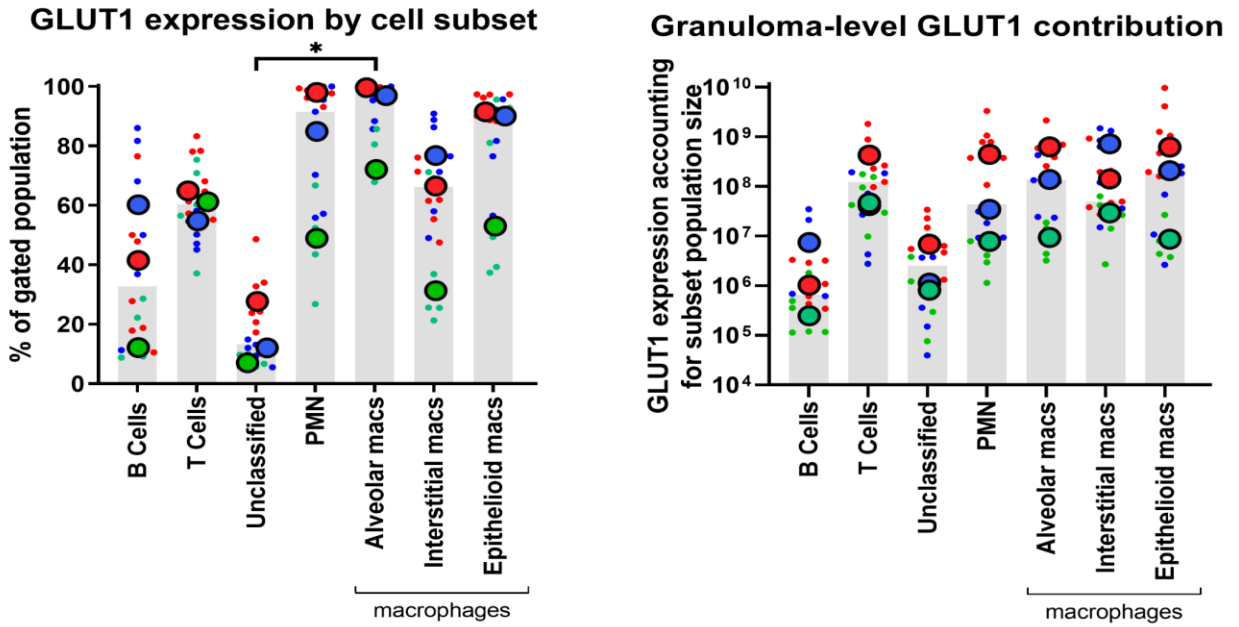

Figure 10. Different cell subsets express variable amounts of GLUT1 in granulomas

(Left) The columns represent the median frequency of GLUT1+ B cells, T cells, unclassified lymphocyte-sized cells, neutrophils (PMN), and macrophage subsets. * indicates $p<0.05$. (Right) Column graphs with bars representing the median overall GLUT1 expression by each cell subset after accounting for population size (GLUT1 index). Individual granulomas are represented by small dots and large dots represent the median of all granulomas from an animal where each animal is represented by a different color.

To get a better sense for how much each population contributes to the overall GLUT1 expression in a granuloma, where we are considering GLUT1 as a proxy for glycolytic metabolism, we calculated a GLUT1 index that accounts for the total number of cells with a population and the overall GLUT1 expression/cell. More so, GLUT1 index took into account

differences in size between cell types and difference in number of cells found in a granuloma of each cell type. We did not find a significant difference when comparing the median GLUT1 index of each NHP (**Figure 10 Right**). The overall GLUT1 expression per granuloma (GLUT1 index) when accounting for cell population size suggests that a granuloma's overall capacity to use glucose is multifactorial and although macrophages may express more GLUT1 on a per cell basis, inflammation driven by large numbers of cells with lower GLUT1 expression can be important contributors to glucose uptake.

3.4 Modeling Glucose Uptake with 2-NBDG

3.4.1 Macrophage 2-NBDG uptake

Cells in different granuloma regions are exposed to variable amounts of bacterial antigen and hypoxia. The effect these conditions have on macrophages cannot be assessed *in vivo* and so we used *in vitro* experiments with monocyte-derived macrophages to model the effect of Mtb exposure or low oxygen conditions on glucose uptake. In order to determine if gamma-radiated *Mtb* (*yMtb*) can stimulate macrophages to uptake glucose, we performed four glucose uptake assays using a glucose analog, fluorescence-labeled 2-deoxyglucose, 2-NBDG, on monocyte-derived macrophages from four different NHPs (M22618, M13618, M21718, and M22118). After taking images, we quantified the mean intensity of 2-NBDG in the cells at 10 minutes, 30 minutes, 1 hour, 3 hour, and overnight timepoints with CellProfiler (**Figure 11**).

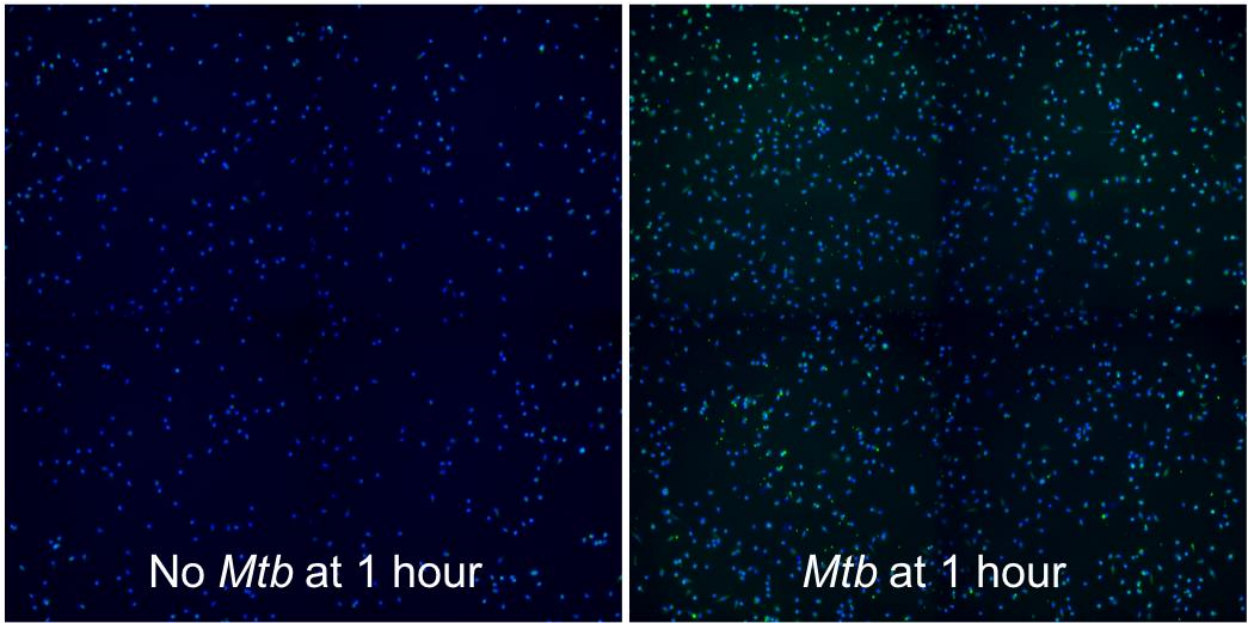

Figure 11. Monocyte derived macrophages take up 2-NBDG after stimulation with Mtb

Microscopy of monocyte-derived macrophages from PBMCs of NHP infected with Mtb that were either stimulated or unstimulated with gamma-radiated Mtb at the 1-hour timepoint. Green fluorescence is 2-NBDG.

There was a significant amount of inter-cell variability within a treatment condition indicating that macrophage glucose uptake is heterogenous within a culture. In **Figure 12 Left,** shows the results from one NHP (M13618) and when the control (no stimulation) and *Mtb*-stimulated cells were compared with a non-parametric T test (Mann Whitney), there was a significant difference between unstimulated and stimulated cells with there being an increase in 2-NBDG uptake occurring within 30 minutes.

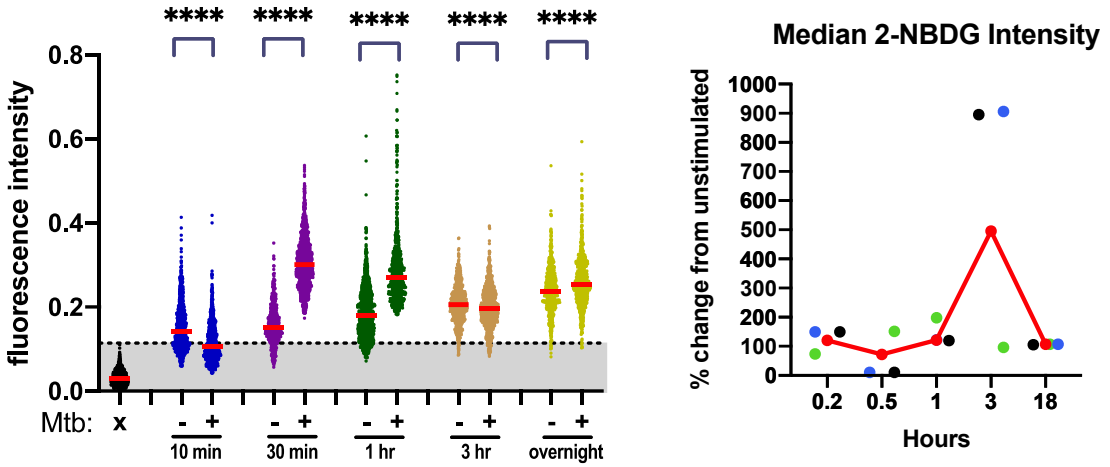

Figure 12. 2-NBDG on monocyte-derived macrophages from PBMCs of NHP infected with Mtb that were either stimulated or unstimulated with gamma-radiated Mtb

(Left) a 2-NBDG uptake assy showing the fluorescence intensity at each timepoint from one NHP (M13618) **(Right)** Comparing the median 2-NBDG intensity of all four glucose uptake assays per NHP (M13618, green; M22618, blue; M22718, grey; M22118, black) and comparing the median 2-NBDG among all four NHP (red).

We normalized the data by calculating the percent change from unstimulated control by dividing the median stimulated MFI by the median unstimulated MFI **(Figure 13, right)**. We then calculated the median of these values for all NHP together, as shown in red (**Figure 13, right**). Overall, these data suggest that macrophages can be activated by exposure to *Mtb* antigen and take up glucose within three hours of stimulation. We also noted substantial variability between animals and speculate this may be attributable to different differences in the number of antigen specific-T cells that are present in the monocyte-derived macrophage cultures after the initial CD14 isolation.

3.4.2 Hypoxic Experiments with 2-NBDG

Cells shift toward glycolytic metabolism to survive in hypoxic environments, and because our IHC-based data suggest that GLUT1+ epithelioid macrophages exist in hypoxic environments, we hypothesized that macrophages in hypoxic environments would take up more glucose (2-

NBDG) than macrophages in normoxic environments. We lack access to a hypoxia chamber that can accommodate BSL2+ nonhuman primate cells, and so to test this hypothesis, we incubated cells in a desiccator where the oxygen had been exhausted by a candle. Rather than analyze the 2-NBDG fluorescence by microscopy, we used flow cytometry to determine if this approach was suitable for this assay. By using flow cytometry, we were able to identify macrophage populations and residual T cells that remained in culture after monocyte isolation and determined the 2-NBDG MFI of these cell populations (**Figure 14).** We can see that for both T cells and macrophages (myeloid gate) that there is a lack of difference between 1 hour and 3 hours in all four of our conditions (hypoxic with stimulation, hypoxic without stimulation, normal with stimulation, and normal without stimulation).

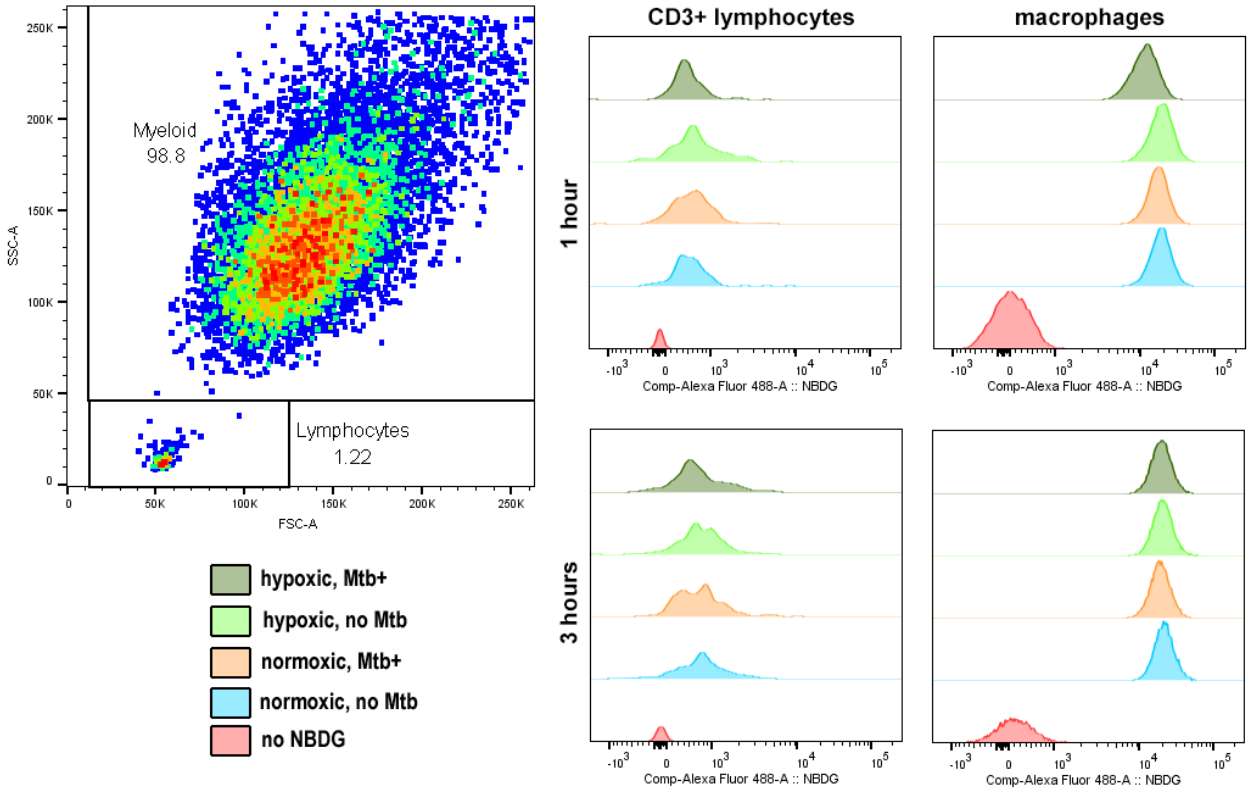

Figure 13. 2-NBDG MFI of CD3+ lymphocytes and CD11b+ macrophages

Comparisons of 2-NBDG MFI for each of our experimental conditions (hypoxic with stimulation, hypoxic without stimulation, normal with stimulation, and normal without stimulation) for T cells and macrophages at 1 hour and 3 hours.

We were able to perform one assay with cells from one animal before being forced to end our experiments because of the COVID-19 pandemic; thus, these data are pilot data to demonstrate proof of concept that this approach can be used for this assay. Because of the limited dataset, we are not making interpretations of this data, but note that monocyte-derived macrophages still contain residual populations of lymphocytes **(Figure 14)** with CD3+ T cells. We found that T cells took up substantially less 2-NBDG than macrophages, but although there appeared to be a trend toward greater 2-NBDG uptake in cells incubated under hypoxia for 3 hours, we did not see an obvious trend that related to exposure to *yMtb* **(Figure 15)**.

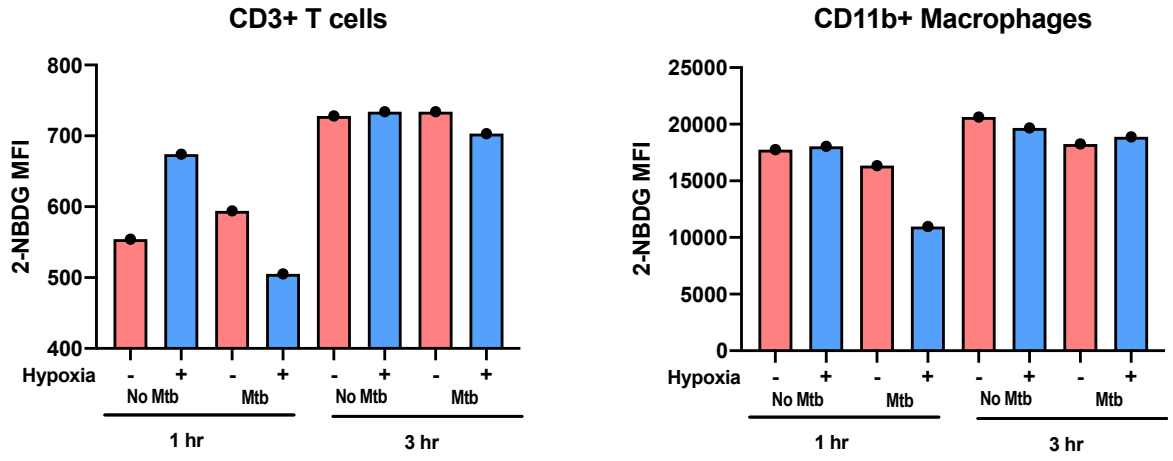

Figure 14. 2-NBDG MFI of CD3+ lymphocytes and CD11b+ macrophages

Comparison of CD3+ T cells and CD11b+ macrophages at 1 and 3 hours that were either stimulated or unstimulated with Mtb in a hypoxic or oxygenated environment.

4.0 Discussion

We used GLUT1 expression as a proxy for glycolytic metabolism in granulomas as well as 2-NBDG with monocyte-derived macrophages to identify the relationship between *Mtb* antigens and macrophage glucose uptake, thus offering mechanistic insights into granuloma biology. My hypothesis was that macrophages in regions of hypoxia or with exposure to *Mtb* antigens will express more GLUT1 as compared to regions of normoxic conditions or lower *Mtb* exposure in lung granulomas. Thus, my specific aims are to 1) identify which cell types in granulomas use glycolysis as their energy source and 2) identify potential drivers of glycolysis in granuloma macrophages.

4.1 Epithelioid Macrophages Express GLUT1 in Lung Granulomas

GLUT1 is a well characterized glucose transporter expressed by leukocytes that has been used as an indicator of immune cell glycolysis metabolism (37). We found a significantly higher proportion of the granuloma area was occupied by GLUT1+ macrophages than GLUT1- macrophages. More so, we found that GLUT1 expression varies among macrophage subsets with epithelioid macrophages expressing more GLUT1 as compared to interstitial and alveolar macrophages. Epithelioid macrophages are likely important contributors to the overall granuloma glucose uptake, since we saw a lack of significant difference between the overall GLUT1 expression and epithelioid macrophages per NHP.

M1 and M2 macrophages differ in immunometabolic responses in the presence of *Mtb* (25). M1 macrophage polarization is characterized by an up-regulation of genes consistent with the Warburg effect (25). M1 macrophages are activated after stimulation with LBS or TLR ligation (25, 39, 40). More so, epithelioid macrophages are near the caseous region of the granuloma, these cells are exposed to *Mtb* antigen as well as in an area of low oxygen. Through these IHC experiments, we can see that epithelioid macrophages act more like M1 macrophages likely due their location within a granuloma. In order to survive in this environment, these cells likely switch from oxidative phosphorylation to glycolysis to generate ATP faster.

Unlike M1 macrophages, M2 macrophages upregulates Arg-1, signal transducer and activator of transcription 6 (STAT6), and GATA binding protein 3 (GATA3) in order to produce anti-inflammatory cytokine IL-10 (25). M2 macrophages have an intact TCA cycle to allow for the generation of ATP through oxidative phosphorylation and concomitantly display increased glycolysis as a carbon source (43, 44). Since interstitial and alveolar macrophages do not express as much GLUT1 as compared to epithelioid, it could indicate that these macrophages are following more of M2 macrophage metabolism or are just not as activated in lung granulomas. More so, these macrophages are located toward the outer areas of the granuloma where there is less *Mtb* antigen and is more oxygenated. From previous studies conducted by Mattila et al. 2013 and from our IHC microscopy, we can see that interstitial and alveolar macrophages are located in the lymphocyte cuff and could be have more anti-inflammatory properties, like M2 macrophages.

Since we found that there was not a significant difference between the overall GLUT1 expression and the sum of the GLUT1+ macrophage expression (per granuloma level), this provides evidence that other immune cells are likely contributing to the overall GLUT1 expression in addition to macrophages.

4.2 T cells, B cells, and Myeloid Cells Express GLUT1 in Lung Granulomas

Enhanced utilization of glycolysis occurs in other immune cells such as dendritic cells (DCs), natural killer cells (NK), and T cells where it is important for rapid replication and high levels of activity including cytokine expression (37). To show that other cells types found in lung granulomas also express GLUT1, we used lung granulomas from NHP infected with *Mtb* and flow cytometry to determine the frequency of GLUT1 and the GLUT1 index of B cells, T cells, neutrophils (PMN), and macrophages. We found that T cells, B cells, neutrophils, and macrophages all express GLUT1 in lung granulomas but macrophages, T cells, and neutrophils (PMN) had a higher frequency of GLUT1 expression and GLUT1 index as compared to B cells and unclassified cells. This supports that that other immune cells in granulomas are contributing to the overall GLUT1 expression in lung granulomas. Macrophages are larger than T cells but there is a larger number of T cells within a granuloma than macrophages. Although we used the GLUT1 index to try to account for these differences, this could still be a reason for the lack of difference in GLUT1 expression between T cells and macrophages.

The flow cytometry data supports the data seen in our IHC experiments that macrophages are highly express GLUT1. As well as support the notion that that along with macrophages, T cells, B cells, and other myeloid cells are activated in lung granulomas and contribute to the overall GLUT1 expression seen in lung granulomas. Overall, we see that macrophages express the most GLUT1 followed by T cells and neutrophils and then B cells and unclassified cells.

4.3 Macrophages are ACTIVATED UPON STIMULATION with *Mtb* Antigen

PET-CT using fluorodeoxyglucose (^{18}F-FDG), a glucose analog, has become an increasingly important tool for diagnosing TB (48) and uncovering the drivers of glucose uptake, as visualized by ^{18}F-FDG PET signal, can be translated into meaningful insight into the development and cellular changes that occur in granulomas. In addition to ^{18}F-FDG, studies have shown that using 2-NBDG, a fluorescent analog of D-glucose, can also be used to as a probe for monitoring glucose uptake in malignant tumor cells (50). By using 2-NBDG, a glucose analog similar to FDG, we can perform experiments that could give insight to the mechanics of glycolysis in monocyte-derived macrophages. In our experiments using 2-NBDG, we found that monocyte-derived macrophages are quickly activated upon stimulation with *yMtb*. This further indicates that upon infection, macrophages are quickly activated and use glycolysis to produce ATP. Although, we also saw that there is a high variation among NHP and requires further analyses to better determine the relationship between *yMtb* stimulation and macrophage activation.

Data from the 2-NBDG assay and the flow cytometry data using the NHP lung granulomas validate the PET-CT images, in that macrophages are likely contributing to the ^{18}F-FDG PET signal. This 2-NBDG data can help to better understand the diagnostic power of PET-CT, as macrophages quickly take up 2-NBDG upon stimulation. We can use ^{18}F-FDG PET-CT in conjunction with 2-NBDG to follow disease progression and treatment outcomes.

4.4 Evidence Toward Hypoxia Effecting 2-NBDG UPTAKE in Macrophages

Glycolysis enables tumor cells to survive and replicate rapidly in normoxic and hypoxic environments (38). Granulomas are poorly vascularized structures that lack nutrients and oxygen, especially at the core of the lesion (54). Macrophages are the most abundant immune cell at the center of granulomas and must adapt to this hypoxic condition, such as using glycolysis to generate more ATP (54). Macrophages increase hypoxia-inducible factor 1-α (HIF1α), which is directly involved in cell growth, differentiation, and survival (54). In normoxic conditions, HIF1α has a short half-life, but under hypoxic conditions, HIF1α becomes transcriptionally active and the classical target genes include glucose transporters (54). HIF1α can also be stimulated by stimuli such as LPS, TBFα, and glucose concentrations in nonhypoxic conditions (54).

Commonly seen in malignant tumors, cells have the ability to increased cellular glycolysis and increase glucose uptake (50). By using glucose analogs, PET CT can be used to create images to identify malignant tumors (50). Although 2-doxy-2-[F-18]fluoro-D-glucose (FDG) is commonly used as the glucose analog for PET CT, studies have shown that another glucose analog, 2-NBDG can also be used as a probe for glucose uptake in malignant cells (50).

Through our experiments using the hypoxic chamber, we saw lack of any evidence that stimulation or hypoxic conditions affect 2-NBDG MFI. We did find that T cells took up substantially less 2-NBDG than macrophages, although there appeared to be a trend toward greater 2-NBDG uptake in cells incubated under hypoxia for 3 hours. We did not see an obvious trend that related to exposure to *yMtb.* Since this was a pilot experiment, it would be useful to repeat this experiment to determine if this is a normal trend. It would also be useful to include HIF1α and GLUT1 cell surface staining to determine if these cells are expressing these cell markers. This

would help conclude if glycolysis and hypoxia are related to each other in macrophages. By further understanding the relationship between macrophage metabolism, HIF1a, and Mtb exposure, we can provide new treatments that could reduce treatment lengths by disrupting metabolism of infected immune cells to reduce *Mtb* dissemination.

4.5 Conclusions

Overall, by looking at each of our methods, we see evidence that macrophages and other cells in lung granulomas express GLUT1 and that macrophages are activated when exposed to *Mtb* antigen. We also found some evidence that macrophages are activated in hypoxic environments, but further experiments are warranted to make any definitive conclusions. We speculate that upon infection, that macrophages, such as epithelioid macrophages, are infected but not fully activated. Once T cells are primed and return, they activate these macrophages. These macrophages then switch to glycolysis, produce chemokine and cytokines to activate other immune cells, and the granuloma forms (3-4 weeks post infection). Around this same time, we are able to use PET-CT to identify these lung granulomas due to macrophages and other immune cells using glycolysis as their energy source and able to take in FDG.

My hypothesis was that macrophages in regions of hypoxia or with exposure to *Mtb* antigens will express more GLUT1 as compared to regions of normoxic conditions or lower *Mtb* exposure in lung granulomas. Thus, my specific aims were to 1) identify which cell types in granulomas use glycolysis as their energy source and 2) identify potential drivers of glycolysis in granuloma macrophages. Through this study, we were able to show evidence of GLUT1 expression, a proxy for glycolysis, in macrophages, T cells, and neutrophils (PMNs) as well as

how that *Mtb* antigen can activate macrophages. We were able to further understand immunometabolism in granulomas and support my hypothesis through my specific aims.

4.6 Public Health Statement

Since we know that macrophages are likely contributors to FDG signal, we can further develop the use of PET-CT with 2-NBDG to help with diagnostics and treatment outcomes. More so, it can give us the ability to better study granuloma formation and disease progression. By understanding immunometabolism in granulomas, we can create therapeutics to help combat *Mtb* infection or reduce duration of treatment to avoid multidrug resistance by directly disrupting infected immune cells metabolism.

4.7 Future Directions

Future directions would conduct experiments to understand the metabolism of *Mtb* and its interaction with the host. More so, granulomas can be formed in other tissues, such as lymph nodes, and would be important to determine if immunometabolism of immune cells in other tissues are similar to the lung. And lastly, further evidence is needed to determine if bacterial burden (CFU) can relate to GLUT1 expression and immunometabolism in granulomas.

Appendix A ImadeJ Macro for Image Analysis

Below is the macro used for image analysis on the lung tissue granulomas to determine the total area and percent area in pixels of GLUT1, CD11c, CD163 individually and in colocalization with one another.

//Create an ROI. Measure area of red, green, blue stain. Measure area of colocalization of stains, with stain not of interest subtrated out (eg. red AND green NOT blue). Count total cells. Count cells that are red AND not green or blue.

```
//area and % area of red
//area  and % area of green
//area  and % area of blue
//area  and % area of red without colocalized green and blue
//area  and % area of red + green colocalization without blue
//area  and % area of red + blue colocalization without green
//area  and % area of red + green + blue colocalization
//area  and % area of blue without colocalized green and red
//area  and % area of red without colocalized red and blue
//area  and % area of blue + green colocalization without red
//Cell Count using DAPI (cells that are red without colocalized green and blue)
```

//THIS MACRO ONLY COUNTS THE NUMBER OF CELLS USING THE DAPI IMAGE. IGNORE THE COUNTS COLUMN IN THE SUMMARY WINDOW FOR ANYTHING LABELED AS 'AREA OF'.

waitForUser("JUST A REMINDER THAT THIS MACRO ONLY COUNTS THE NUMBER OF CELLS USING THE DAPI IMAGE. IGNORE THE COUNTS COLUMN IN THE SUMMARY WINDOW FOR ANYTHING LABELED AS 'AREA OF'. Click OK to continue");

waitForUser("Open DAPI Image. Wait for image to open and then click OK")
waitForUser("Draw ROI, click Ctrl + t, then click OK"); create region of interest and add that region to the ROI manager.
run("Clear Outside"); remove any part of the DAPI image that is not contained within the ROI.
rename("DAPI") rename the current image

waitForUser("Open RGB Image. Wait for image to open and then click OK")
roiManager("Select", 0); select the first ROI in the ROI manager and apply to the RGB image

setBackgroundColor(0, 0, 0); [I'm guessing this is to choose the color black]
run("Clear Outside"); remove any part of the RGB image that is not contained within the ROI.

waitForUser("Click More on ROI Manager window and save the ROI as an overlay,then click OK")

currentTitle = getTitle(); retrieve the file name
run("Split Channels"); split the RGB image into red, green, and blue individual images
greenTitle = currentTitle + " (green)"; name green image with file name and green
redTitle = currentTitle + " (red)"; name red image with file name and red
blueTitle = currentTitle + " (blue)"; name blue image with file name and blue

selectWindow(redTitle); select red image
run("Duplicate...", "redTitle") duplicate the red image so that the original image can be used twice in this macro
rename(redTitle + " area of red") rename duplicate image with file name and area of red
setAutoThreshold("Default"); open threshold with default settings
run("Threshold..."); a threshold range is set to tell the objects of interest apart from the background
waitForUser("Set the threshold by using the slider (DO NOT click Apply) then click OK"); allow user to set the threshold manually
setOption("BlackBackground", false); apply the threshold to the image
run("Convert to Mask"); converts the image to black and white based on the current threshold settings; this is now an 8-bit image
run("Close"); close the threshold window
run("Invert"); pixels that are currently displayed as white will become black, and vice versa
roiManager("Select", 0); select the first ROI in the ROI manager and apply to the current image
run("Analyze Particles...", "size=0-Infinity show=Overlay display summarize in_situ"); select the particles that are sized between zero and infinity; for the particles that are selected draw a line around them; display data in the results table; put the info for the particles into the summary table; open the resulting image with the overlay in a new window
run("Invert"); pixels that are currently displayed as white will become black, and vice versa
run("RGB Color"); this will change the image from an 8-bit image to an RGB image

selectWindow(greenTitle);
run("Duplicate...", "greenTitle")
rename(greenTitle + " area of green")
setAutoThreshold("Default");
run("Threshold...");
waitForUser("Set the threshold by using the slider (DO NOT click Apply) then click OK");
setOption("BlackBackground", false);
run("Convert to Mask");

```
run("Invert");
roiManager("Select", 0);
run("Analyze Particles...", "size=0-Infinity show=Overlay display summarize in_situ");
run("Invert");
run("RGB Color");

selectWindow(blueTitle);
run("Duplicate...", "blueTitle")
rename(blueTitle + " area of blue")
setAutoThreshold("Default");
run("Threshold...");
waitForUser("Set the threshold by using the slider (DO NOT click Apply) then click OK");
setOption("BlackBackground", false);
run("Convert to Mask");
run("Close");
run("Invert");
roiManager("Select", 0);
run("Analyze Particles...", "size=0-Infinity show=Overlay display summarize in_situ");
run("Invert");
run("RGB Color");

imageCalculator("Subtract create", redTitle + " area of red", greenTitle + " area of green");
remove any area of the image that is in both the images and create a new image
rename("area of red - area of green")
imageCalculator("Subtract create", "area of red - area of green", blueTitle + " area of blue");
run("8-bit"); change the image to an 8-bit image
run("Invert");
rename(redTitle + " area of red without colocalized green and blue")
roiManager("Select", 0);
run("Analyze Particles...", "size=0-Infinity   show=Overlay display summarize in_situ");
run("Invert");
run("RGB Color");


imageCalculator("AND create", redTitle + " area of red", greenTitle + " area of green");
keep only the parts of the two images that overlap and create a new image
rename("area of red + area of green")
imageCalculator("Subtract create", "area of red + area of green", blueTitle + " area of blue");
run("8-bit");
run("Invert");
rename(redTitle + " area of red + green colocalization without blue")
roiManager("Select", 0);
run("Analyze Particles...", "size=0-Infinity   show=Overlay display summarize in_situ");
```

```
imageCalculator("AND create", redTitle + " area of red", blueTitle + " area of blue");
rename("area of red + area of blue")
imageCalculator("Subtract create", "area of red + area of blue", greenTitle + " area of green");
run("8-bit");
run("Invert");
rename(redTitle + " area of red + blue colocalization without green")
roiManager("Select", 0);
run("Analyze Particles...", "size=0-Infinity   show=Overlay display summarize in_situ");


imageCalculator("AND create", "area of red + area of blue", greenTitle + " area of green");
run("8-bit");
run("Invert");
rename(redTitle + " area of red + green + blue colocalization")
roiManager("Select", 0);
run("Analyze Particles...", "size=0-Infinity   show=Overlay display summarize in_situ");

imageCalculator("Subtract create", blueTitle + " area of blue", greenTitle + " area of green");
rename("area of blue - area of green")
imageCalculator("Subtract create", "area of blue - area of green", redTitle + " area of red");
run("8-bit");
run("Invert");
rename(blueTitle + " area of blue without colocalized green and red")
roiManager("Select", 0);
run("Analyze Particles...", "size=0-Infinity   show=Overlay display summarize in_situ");

imageCalculator("Subtract create", greenTitle + " area of green", redTitle + " area of red");
rename("area of green - area of red")
imageCalculator("Subtract create", "area of green - area of red", blueTitle + " area of blue");
run("8-bit");
run("Invert");
rename(greenTitle + " area of green without colocalized red and blue")
roiManager("Select", 0);
run("Analyze Particles...", "size=0-Infinity   show=Overlay display summarize in_situ");

imageCalculator("AND create", blueTitle + " area of blue", greenTitle + " area of green");
rename("area of blue + area of green")
imageCalculator("Subtract create", "area of blue + area of green", redTitle + " area of red");
run("8-bit");
run("Invert");
rename(blueTitle + " area of blue + green colocalization without red")
roiManager("Select", 0);
```

```
run("Analyze Particles...", "size=0-Infinity   show=Overlay display summarize in_situ");

selectWindow("DAPI");
rename("Cell Count using DAPI")
run("8-bit");
setAutoThreshold("Default");
run("Threshold...");
waitForUser("Set the threshold (DO NOT click Apply), then click OK");
run("Close");
setOption("BlackBackground", false);
run("Convert to Mask");
run("Invert");
run("Watershed"); used to segment objects
roiManager("Select", 0);
run("Analyze Particles...", "size=10-infinity show=Overlay display summarize add in_situ"); the “add” in this step will add each particle to the ROI Manager as an individual ROI
run("Fill Holes") fill in any “holes” that are in objects to make them solid
run("Watershed");
run("Invert");
run("RGB Color");

roiManager("Select", 0);
roiManager("Delete"); delete the first ROI, the one that was created at the beginning of this macro
close("Results") close the results window so the new data will not get added onto the end of the previous data

imageCalculator("AND create", "Cell Count using DAPI", redTitle + " area of red without colocalized green and blue");
rename(redTitle + " Cell Count of red without green and blue colocalization, using DAPI")
close("Results")
run("8-bit");
setAutoThreshold("Default");
run("Threshold...");
setOption("BlackBackground", false);
run("Convert to Mask");
run("Invert");

roiManager("Show All"); this is just so the ROI Manager window is selected
roiManager("Measure"); measure and record the data for each individual ROI that was created in the above analyze particle step (from the DAPI image)

waitForUser("Copy Summary and Results and paste into Excel. Sort the Results and count # of objects that are not zero or 255, that is your # of cells that are also red (without colocalized green and blue). When ready to close all, click OK");
```

The rest of these steps will just close all of the open windows.

```
selectWindow("ROI Manager");
run("Close");
selectWindow("Threshold");
run("Close");

close("Results")
close("Log")
run("Close All");
close("Summary")
```

Appendix B NBDG Chemical Formulation

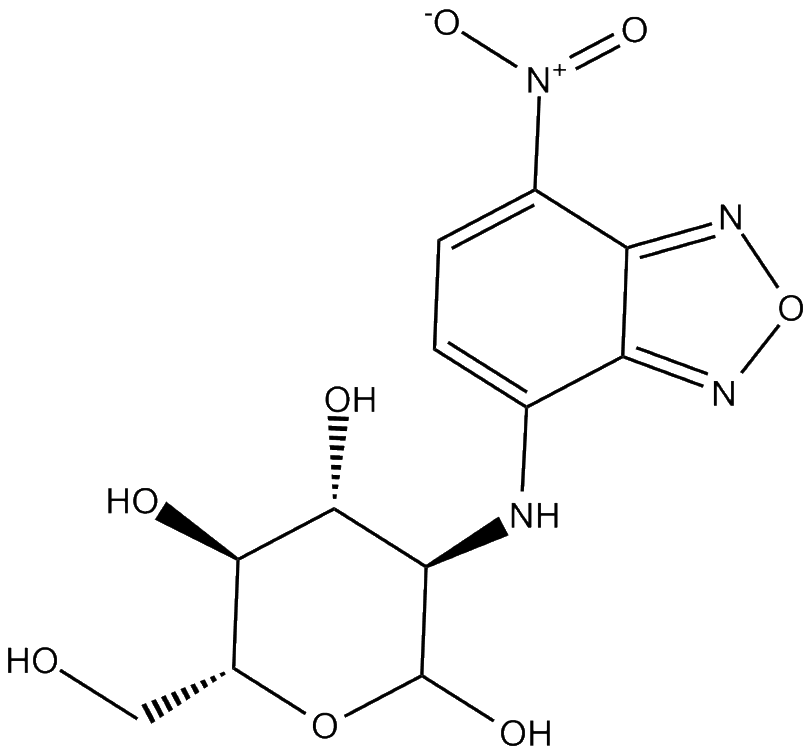

Bibliography

1. Shi L, Eugenin EA, Subbian S. 2016. Immunometabolism in tuberculosis. Frontiers in immunology 7:150.
2. Dong H, Lv Y, Sreevatsan S, Zhao D, Zhou X. 2017. Differences in pathogenicity of three animal isolates of Mycobacterium species in a mouse model. PloS one 12.
3. Boire NA, Riedel VAA, Parrish NM, Riedel S. 2013. Tuberculosis: from an untreatable disease in antiquity to an untreatable disease in modern times. J Anc Dis Prev Rem 1:1-11.
4. Ulrichs T. 2012. How tuberculosis influenced history-and vice versa. Pneumologie (Stuttgart, Germany) 66:59-66.
5. Maulitz RC, Maulitz SR. 1973. The king's evil in Oxfordshire. Medical history 17:87-89.
6. Millet J-P, Moreno A, Fina L, Del Baño L, Orcau A, De Olalla PG, Cayla JA. 2013. Factors that influence current tuberculosis epidemiology. European Spine Journal 22:539-548.
7. Kochi A. 2001. The global tuberculosis situation and the new control strategy of the World Health Organization. SciELO Public Health.
8. Sharma S, Mohan A, Kadhiravan T. 2005. HIV-TB co-infection: epidemiology, diagnosis & management. Indian J Med Res 121:550-567.
9. Sandhu G, Battaglia F, Ely BK, Athanasakis D, Montoya R, Valencia T, Gilman RH, Evans CA, Friedland JS, Fernandez-Reyes D. 2012. Discriminating active from latent tuberculosis in patients presenting to community clinics. PLoS One 7.
10. Chen C, Zhu T, Wang Z, Peng H, Kong W, Zhou Y, Shao Y, Zhu L, Lu W. 2015. High latent TB infection rate and associated risk factors in the Eastern China of low TB incidence. PLOS one 10.
11. Patra J, Jha P, Rehm J, Suraweera W. 2014. Tobacco smoking, alcohol drinking, diabetes, low body mass index and the risk of self-reported symptoms of active tuberculosis: individual participant data (IPD) meta-analyses of 72,684 individuals in 14 high tuberculosis burden countries. PloS one 9.
12. Banuls A-L, Sanou A, Van Anh NT, Godreuil S. 2015. Mycobacterium tuberculosis: ecology and evolution of a human bacterium. Journal of medical microbiology 64:1261-1269.
13. Ai J-W, Ruan Q-L, Liu Q-H, Zhang W-H. 2016. Updates on the risk factors for latent tuberculosis reactivation and their managements. Emerging microbes & infections 5:1-8.
14. Sia IG, Wieland ML. Current concepts in the management of tuberculosis, p 348-361. *In* (ed), Elsevier,
15. Salgame P, Geadas C, Collins L, Jones-López E, Ellner JJ. 2015. Latent tuberculosis infection–revisiting and revising concepts. Tuberculosis 95:373-384.
16. Kaul KL. 2001. Molecular detection of Mycobacterium tuberculosis: impact on patient care. Clinical chemistry 47:1553-1558.
17. Prevention CfDCa. 2009. Updated guidelines for the use of nucleic acid amplification tests in the diagnosis of tuberculosis. https://www.cdc.gov/mmwr/preview/mmwrhtml/mm5801a3.htm. Accessed 1.
18. Zumla A, Nahid P, Cole ST. 2013. Advances in the development of new tuberculosis drugs and treatment regimens. Nature reviews Drug discovery 12:388-404.

19. Luca S, Mihaescu T. 2013. History of BCG Vaccine. Maedica 8:53-58.
20. Rodrigues LC, Diwan VK, Wheeler JG. 1993. Protective effect of BCG against tuberculous meningitis and miliary tuberculosis: a meta-analysis. International journal of epidemiology 22:1154-1158.
21. Nguipdop-Djomo P, Heldal E, Rodrigues LC, Abubakar I, Mangtani P. 2016. Duration of BCG protection against tuberculosis and change in effectiveness with time since vaccination in Norway: a retrospective population-based cohort study. The Lancet infectious diseases 16:219-226.
22. Suliman S, Geldenhuys H, Johnson JL, Hughes JE, Smit E, Murphy M, Toefy A, Lerumo L, Hopley C, Pienaar B. 2016. Bacillus Calmette–Guerin (BCG) revaccination of adults with latent Mycobacterium tuberculosis infection induces long-lived BCG-reactive NK cell responses. The Journal of Immunology 197:1100-1110.
23. Darrah PA, Zeppa JJ, Maiello P, Hackney JA, Wadsworth MH, Hughes TK, Pokkali S, Swanson PA, Grant NL, Rodgers MA. 2020. Prevention of tuberculosis in macaques after intravenous BCG immunization. Nature 577:95-102.
24. Young D. 2009. Animal models of tuberculosis. European journal of immunology 39:2011-2014.
25. Wilson JL, Mayr H, Weichhart T. 2019. Metabolic Programming of Macrophages: Implications in the Pathogenesis of Granulomatous Disease. Frontiers in immunology 10:2265.
26. Mattila JT, Beaino W, Maiello PA, Coleman MT, White AG, Scanga CA, Flynn JL, Anderson CJ. 2017. PET imaging of macaques with tuberculosis identifies temporal changes in granuloma glucose metabolism and integrin α4β1-expressing immune cells. Journal of immunology (Baltimore, Md: 1950) 199:806.
27. Rothchild AC, Olson GS, Nemeth J, Amon LM, Mai D, Gold ES, Diercks AH, Aderem A. 2019. Alveolar macrophages up-regulate a non-classical innate response to Mycobacterium tuberculosis infection in vivo. bioRxiv:520791.
28. Awuh JA, Flo TH. 2017. Molecular basis of mycobacterial survival in macrophages. Cellular and Molecular Life Sciences 74:1625-1648.
29. Olive AJ, Sassetti CM. 2018. Tolerating the unwelcome guest; how the host withstands persistent Mycobacterium tuberculosis. Frontiers in immunology 9:2094.
30. Srivastava S, Grace PS, Ernst JD. 2016. Antigen export reduces antigen presentation and limits T cell control of M. tuberculosis. Cell host & microbe 19:44-54.
31. Flynn J, Capuano S, Croix D, Pawar S, Myers A, Zinovik A, Klein E. 2003. Non-human primates: a model for tuberculosis research. Tuberculosis 83:116-118.
32. Mattila JT, Ojo OO, Kepka-Lenhart D, Marino S, Kim JH, Eum SY, Via LE, Barry CE, Klein E, Kirschner DE. 2013. Microenvironments in tuberculous granulomas are delineated by distinct populations of macrophage subsets and expression of nitric oxide synthase and arginase isoforms. The Journal of Immunology 191:773-784.
33. Lin PL, Ford CB, Coleman MT, Myers AJ, Gawande R, Ioerger T, Sacchettini J, Fortune SM, Flynn JL. 2014. Sterilization of granulomas is common in active and latent tuberculosis despite within-host variability in bacterial killing. Nature medicine 20:75.
34. Kumar R, Singh P, Kolloli A, Shi L, Bushkin Y, Tyagi S, Subbian S. 2019. Immunometabolism of phagocytes during Mycobacterium tuberculosis infection. Frontiers in molecular biosciences 6:105.

35. Rath M, Müller I, Kropf P, Closs EI, Munder M. 2014. Metabolism via arginase or nitric oxide synthase: two competing arginine pathways in macrophages. Frontiers in immunology 5:532.
36. Huang Z, Luo Q, Guo Y, Chen J, Xiong G, Peng Y, Ye J, Li J. 2015. Mycobacterium tuberculosis-induced polarization of human macrophage orchestrates the formation and development of tuberculous granulomas in vitro. PloS one 10.
37. O'Neill LA, Kishton RJ, Rathmell J. 2016. A guide to immunometabolism for immunologists. Nature Reviews Immunology 16:553.
38. Warburg O, Wind F, Negelein E. 1927. The metabolism of tumors in the body. The Journal of general physiology 8:519.
39. Tannahill G, Curtis A, Adamik J, Palsson-McDermott E, McGettrick A, Goel G, Frezza C, Bernard N, Kelly B, Foley N. 2013. Succinate is an inflammatory signal that induces IL-1β through HIF-1α. Nature 496:238-242.
40. Wang L, Hong Y, Wu J, Leung Y-K, Huang Y. 2017. Efficacy of thalidomide therapy in pediatric Crohn's disease with evidence of tuberculosis. World journal of gastroenterology 23:7727.
41. Wei L, Vahedi G, Sun H-W, Watford WT, Takatori H, Ramos HL, Takahashi H, Liang J, Gutierrez-Cruz G, Zang C. 2010. Discrete roles of STAT4 and STAT6 transcription factors in tuning epigenetic modifications and transcription during T helper cell differentiation. Immunity 32:840-851.
42. Zhong Y, Yi C. 2016. MicroRNA-720 suppresses M2 macrophage polarization by targeting GATA3. Bioscience reports 36.
43. Huang SC-C, Everts B, Ivanova Y, O'sullivan D, Nascimento M, Smith AM, Beatty W, Love-Gregory L, Lam WY, O'neill CM. 2014. Cell-intrinsic lysosomal lipolysis is essential for alternative activation of macrophages. Nature immunology 15:846.
44. Linke M, Pham HTT, Katholnig K, Schnöller T, Miller A, Demel F, Schütz B, Rosner M, Kovacic B, Sukhbaatar N. 2017. Chronic signaling via the metabolic checkpoint kinase mTORC1 induces macrophage granuloma formation and marks sarcoidosis progression. Nature immunology 18:293-302.
45. Krzeslak A, Wojcik-Krowiranda K, Forma E, Jozwiak P, Romanowicz H, Bienkiewicz A, Brys M. 2012. Expression of GLUT1 and GLUT3 glucose transporters in endometrial and breast cancers. Pathology & Oncology Research 18:721-728.
46. Deng D, Xu C, Sun P, Wu J, Yan C, Hu M, Yan N. 2014. Crystal structure of the human glucose transporter GLUT1. Nature 510:121-125.
47. Ganapathy-Kanniappan S, Geschwind J-FH. 2013. Tumor glycolysis as a target for cancer therapy: progress and prospects. Molecular cancer 12:152.
48. Vorster M, Sathekge MM, Bomanji J. 2014. Advances in imaging of tuberculosis: the role of 18F-FDG PET and PET/CT. Current opinion in pulmonary medicine 20:287-293.
49. Avril N. 2004. GLUT1 expression in tissue and 18F-FDG uptake. Journal of Nuclear Medicine 45:930-932.
50. O'Neil RG, Wu L, Mullani N. 2005. Uptake of a fluorescent deoxyglucose analog (2-NBDG) in tumor cells. Molecular Imaging and Biology 7:388-392.
51. Via LE, Lin PL, Ray SM, Carrillo J, Allen SS, Eum SY, Taylor K, Klein E, Manjunatha U, Gonzales J. 2008. Tuberculous granulomas are hypoxic in guinea pigs, rabbits, and nonhuman primates. Infection and immunity 76:2333-2340.

52. Green AM, Mattila JT, Bigbee CL, Bongers KS, Ling Lin P, Flynn JL. 2010. CD4+ regulatory T cells in a cynomolgus macaque model of Mycobacterium tuberculosis infection. The Journal of infectious diseases 202:533-541.
53. Rice G. 2019. Fluorescent Microscopy, *on* Microbial Life Education Resources. https://serc.carleton.edu/microbelife/research_methods/microscopy/fluromic.html. Accessed
54. Cardoso MS, Silva TM, Resende M, Appelberg R, Borges M. 2015. Lack of the transcription factor hypoxia-inducible factor 1α (HIF-1α) in macrophages accelerates the necrosis of Mycobacterium avium-induced granulomas. Infection and immunity 83:3534-3544.